PHYSICAL REVIEW D **78,** 064040 (2008)

Phenomenological loop quantum geometry of the Schwarzschild black hole

Dah-Wei Chiou*

Institute for Gravitation and the Cosmos, Physics Department, The Pennsylvania State University, University Park, Pennsylvania 16802, USA

(Received 10 July 2008; published 15 September 2008)

The interior of a Schwarzschild black hole is investigated at the level of phenomenological dynamics with the discreteness corrections of loop quantum geometry implemented in two different improved quantization schemes. In one scheme, the classical black hole singularity is resolved by the quantum bounce, which bridges the black hole interior with a white hole interior. In the other scheme, the classical singularity is resolved and the event horizon is also diffused by the quantum bounce. Jumping over the quantum bounce, the black hole gives birth to a baby black hole with a much smaller mass. This lineage continues as each classical black hole brings forth its own descendant in the consecutive classical cycle, giving the whole extended spacetime fractal structure, until the solution eventually descends into the deep Planck regime, signaling a breakdown of the semiclassical description. The issues of scaling symmetry and no-hair theorem are also discussed.

DOI: 10.1103/PhysRevD.78.064040 PACS numbers: 04.60.Pp, 03.65.Sq, 04.70.Dy, 98.80.Qc

I. INTRODUCTION

It has long been suggested that the singularities in general relativity signal a breakdown of the classical theory and should be resolved by the quantum effects of gravity. Loop quantum gravity (LQG) is one of such candidate theories of quantum gravity and its application to cosmological models is known as loop quantum cosmology (LQC) (see [1] for a review). The comprehensive formulation for LQC has been constructed in detail in the spatially flat and isotropic model with a free massless scalar field [2–4], showing that the quantum evolution is deterministic across the deep Planck regime and the cosmological singularity is replaced by a quantum bounce for the states which are semiclassical at late times. This construction was extended to $k = \pm 1$ Friedmann-Robertson-Walker models to include intrinsic curvature [5,6] as well as Bianchi I models to include anisotropy [7–10], affirming the resolution of cosmological singularities and the occurrence of quantum bounces, either in the fundamental quantum theory of LQC or at the level of phenomenological dynamics.

To further extend this formulation and enlarge its domain of validity, the next step is to investigate loop quantum geometry of the black hole and to see whether the black hole singularity is also resolved. The simplest step is to consider the interior of a Schwarzschild black hole, in which the temporal and radial coordinates flip roles and thus the metric components are homogeneous with the Kantowski-Sachs symmetry. Thanks to homogeneity, the loop quantization of the Schwarzschild interior can be formulated as a minisuperspace model in a similar fashion to LQC. This has been developed in [11–13] and its phenomenological dynamics studied in [14] shows that the black hole interior is extended to a white hole interior through the bounce, which resolves the singularity.

The analysis in [14] is based on the original quantization strategy (referred to as the "μ_o scheme" in this paper) used in [12], which, as a direct transcription of the original LQC construction in [2], introduces a fixed parameter to impose fundamental discreteness of quantum geometry. However, it has been argued that the μ_o-scheme quantization in LQC leads to a wrong semiclassical limit in some regimes and should be improved by replacing the discreteness parameters with adaptive variables which depend on the scale factors [4]. Two improved strategies (called "$\bar{\mu}$ scheme" and "$\bar{\mu}'$ scheme" in this paper) for loop quantization of the Schwarzschild interior were investigated in [15] at the level of phenomenological dynamics.

However, the results of [15] are not easily compared with the bouncing scenario of LQC as some details are still missing. For instance, the exact condition for the occurrence of the bounce has yet to be pinpointed. To have a better understanding of the extended Schwarzschild solution, more effort is needed to investigate the quantum corrections on the horizon and the evolution of the parameters (e.g., mass of the black hole) that characterize different classical phases across the quantum bounce.

In order to bridge the gap between the loop quantum dynamics of cosmological models and that of Schwarzschild black holes, a cosmological model of Kantowski-Sachs spacetime with a massless scalar field has been studied in [16] at the level of phenomenological dynamics. The study of [16] not only sets a new cosmological model of LQC with inclusion of both intrinsic curvature and anisotropy but also facilitates a methodology to study the details of loop quantum geometry of the Schwarzschild interior. By exploiting the methods introduced in [16], we are able to articulate the geometrical

*chiou@gravity.psu.edu

interpretation of the extended Schwarzschild solution and refine some observations obtained in [15].

Based on the same semiclassical approach of [16] to incorporate loop quantum corrections, the phenomenological dynamics of the Schwarzschild interior is investigated in this paper with two improved quantization strategies ($\bar{\mu}$ and $\bar{\mu}'$ schemes). In the $\bar{\mu}$ scheme, the classical singularity is resolved and replaced by the quantum bounce, which bridges the black hole interior with the interior of a white hole. On the other hand, in the $\bar{\mu}'$ scheme, the classical black hole singularity is resolved and the event horizon is diffused by the quantum bounce, across which, the classical black hole gives birth to a baby black hole with a decreased mass in the consecutive classical cycle. This lineage continues, giving the extended spacetime "fractal" structure, until eventually the triad variable p_b grows exponentially while the other triad variable p_c descends into a deep Planck regime, signaling a breakdown of the semiclassical description.

As in the Hamiltonian framework for homogeneous models, we have to restrict the spatial integration to a finite sized shell $\mathcal{I} \times S^2$ to make the Hamiltonian finite. This prescription raises the question whether the resulting dynamics is independent of the choice of $\mathcal{I}$. It can be shown that the phenomenological dynamics in the $\bar{\mu}'$ scheme is completely independent of the choice of $\mathcal{I}$ as is the classical dynamics, while the phenomenological dynamics in the $\bar{\mu}$ scheme reacts to $\mathcal{I}$ and thus, in the language of the "no-hair" theorem, one extra parameter (mass of the conjoined white hole) is required to completely characterize the extended Schwarzschild solution.

In addition to the issues related to the dependence on $\mathcal{I}$, the phenomenological dynamics also reveals interesting scaling symmetry, which is suggestive that the fundamental scale (area gap) imposed for the spatial geometry may give rise to a fundamental scale in temporal measurement.

This paper follows the steps in [16] as closely as possible and uses the same notations thereof.[1] In Sec. II, the Ashtekar variables with the Kantowski-Sachs symmetry are introduced and the classical geometry of the Schwarzschild interior is solved in Hamiltonian formalism. The phenomenological dynamics with discreteness corrections of loop quantum geometry is constructed and solved in Sec. III for the $\bar{\mu}$ and $\bar{\mu}'$ schemes, respectively. The scaling symmetry and related issues are discussed in Sec. IV. Finally, the results are summarized and discussed in Sec. V. For comparison, the phenomenological dynamics in the μ_o scheme is also included in the Appendix.

II. CLASSICAL DYNAMICS

In this section, we first briefly describe the Ashtekar variables for the geometry invariant under the Kantowski-Sachs symmetry [12]. In the Hamiltonian framework, we then solve the classical solution in terms of Ashtekar variables for the interior of a Schwarzschild black hole.

A. Ashtekar variables with the Kantowski-Sachs symmetry

The metric of homogeneous spacetime with the Kantowski-Sachs symmetry group $\mathbb{R} \times SO(3)$ is given by the line element:

$$\begin{aligned} ds^2 &= -d\tau^2 + g_{xx}(\tau)dx^2 + g_{\Omega\Omega}(\tau)d\Omega^2 \\ &= -N(t)^2dt^2 + g_{xx}(t)dx^2 + g_{\theta\theta}(t)d\theta^2 + g_{\phi\phi}(t)d\phi^2, \end{aligned} \tag{2.1}$$

where τ is the proper time, $N(t)$ is the lapse function associated with the arbitrary coordinate time t via $N(t)dt = d\tau$, and $d\Omega^2$ represents the unit 2-sphere given in polar coordinates as

$$d\Omega^2 = d\theta^2 + \sin^2\theta d\phi^2. \tag{2.2}$$

The topology of the homogeneous spatial slices is $\Sigma = \mathbb{R} \times S^2$, which is coordinatized by $x \in \mathbb{R}$, $\theta \in [0, \pi]$, and $\phi \in [0, 2\pi]$.

As in any homogeneous cosmological models, on the homogeneous spacelike slice Σ, we can choose a fiducial triad field of vectors ${}^o e^a_i$ and a fiducial cotriad field of covectors ${}^o\omega^i_a$ that are left-invariant by the action of the Killing fields of Σ. (Note ${}^o e^a_i {}^o\omega^i_b = \delta^a_b$.) The *fiducial* 3-metric of Σ is given by the cotriad ${}^o\omega^i_a$:

$${}^o q_{ab} = {}^o\omega^i_a {}^o\omega^j_b \delta_{ij}. \tag{2.3}$$

In the *comoving coordinates* (x, θ, ϕ), we can choose ${}^o q_{ab}$ to have

$${}^o q_{ab} dx^a dx^b = dx^2 + d\theta^2 + \sin^2\theta d\phi^2, \tag{2.4}$$

which gives ${}^o q := \det {}^o q_{ab} = \sin^2\theta$.

In connection dynamics, the canonical pair consists of the Ashtekar variables: the densitized triads $\tilde{E}^a{}_i(\vec{x})$ and connections $A_a{}^i(\vec{x})$, which satisfy the canonical relation:

$$\{A_a{}^i(\vec{x}), \tilde{E}^b{}_j(\vec{x}')\} = 8\pi G\gamma \delta^i_j \delta^b_a \delta^3(\vec{x} - \vec{x}'), \tag{2.5}$$

where γ is the Barbero-Immirzi parameter. In the case that connections and triads admit the Kantowski-Sachs symmetry $\mathbb{R} \times SO(3)$, $A_a{}^i$ and $\tilde{E}^a{}_i$ after gauge fixing of the Gauss constraint are of the form [12]:

$$\begin{aligned} A &= A_a{}^i \tau_i dx^a \\ &= \tilde{c}\tau_3 dx + \tilde{b}\tau_2 d\theta - \tilde{b}\tau_1 \sin\theta d\phi + \tau_3 \cos\theta d\phi, \end{aligned} \tag{2.6}$$

$$\tilde{E} = \tilde{E}^a{}_i \tau_i \partial_a = \tilde{p}_c \tau_3 \sin\theta \partial_x + \tilde{p}_b \tau_2 \sin\theta \partial_\theta - \tilde{p}_b \tau_1 \partial_\phi, \tag{2.7}$$

where $\tilde{b}$, $\tilde{c}$, $\tilde{p}_b$, and $\tilde{p}_c$ are functions of time only and

[1] Assiduous readers are encouraged to look at [10,16] to see the close parallels.

$\tau_i = -i\sigma_i/2$ are $SU(2)$ generators satisfying $[\tau_i, \tau_i] = \epsilon_{ij}{}^k \tau_k$ (with σ_i being the Pauli matrices).

The symplectic structure on the symmetry-reduced phase space is given by the complete symplectic structure [as in (2.5)] integrated over the finite sized shell $\mathcal{I} \times S^2$:

$$\tilde{\mathbf{\Omega}} = \frac{1}{8\pi G\gamma} \int_{\mathcal{I}\times S^2} d^3x dA_a{}^i(\vec{x}) \wedge d\tilde{E}^a{}_i(\vec{x}) = \frac{L}{2G\gamma}(d\tilde{c} \wedge d\tilde{p}_c + 2d\tilde{b} \wedge d\tilde{p}_b), \tag{2.8}$$

where the integration is over $\theta \in [0, \pi]$, $\phi \in [0, 2\pi]$ and restricted to $x \in \mathcal{I} := [0, L]$; the finite interval $\mathcal{I}$ is prescribed to circumvent the problem due to homogeneity that the spatial integration over the whole spatial slice $\mathbb{R} \times S^2$ diverges. (We will see that this prescription does not change the classical dynamics but might have effects on the quantum corrections.) The reduced symplectic form leads to the canonical relations for the reduced canonical variables:

$$\{\tilde{b}, \tilde{p}_b\} = G\gamma L^{-1}, \qquad \{\tilde{c}, \tilde{p}_c\} = 2G\gamma L^{-1} \tag{2.9}$$

and $\{\tilde{b}, \tilde{c}\} = \{\tilde{p}_b, \tilde{p}_c\} = 0$. It is convenient to introduce the rescaled variables:

$$b := \tilde{b}, \qquad c := L\tilde{c}, \qquad p_b := L\tilde{p}_b, \qquad p_c := \tilde{p}_c, \tag{2.10}$$

which satisfy the canonical relations:

$$\{b, p_b\} = G\gamma, \qquad \{c, p_c\} = 2G\gamma. \tag{2.11}$$

The relation between the densitized triad and the 3-metric is given by

$$qq^{ab} = \delta^{ij}\tilde{E}^a{}_i\tilde{E}^b{}_j, \tag{2.12}$$

which leads to

$$g_{\Omega\Omega} = g_{\theta\theta} = g_{\phi\phi}\sin^2\theta = p_c, \qquad g_{xx} = \frac{p_b^2}{L^2 p_c}. \tag{2.13}$$

Let $S_{x\phi}$, $S_{x\theta}$, and $S_{\theta\phi}$ be the three surfaces of interest, respectively, bounded by the interval $\mathcal{I}$ and the equator, $\mathcal{I}$ and a great circle along a longitude, and the equator and a longitude (so that $S_{\theta\phi}$ forms a quarter of the sphere S^2). It follows that the physical areas of $S_{x\phi}$, $S_{x\theta}$, and $S_{\theta\phi}$ are given by

$$\begin{aligned} \mathbf{A}_{x\phi} &= \mathbf{A}_{x\theta} = 2\pi L\sqrt{g_{xx}g_{\Omega\Omega}} = 2\pi p_b, \\ \mathbf{A}_{\theta\phi} &= \pi g_{\Omega\Omega} = \pi p_c, \end{aligned} \tag{2.14}$$

and the physical volume of $\mathcal{I} \times S^2$ is

$$\mathbf{V} = 4\pi L\sqrt{g_{xx}}g_{\Omega\Omega} = 4\pi p_b\sqrt{p_c}. \tag{2.15}$$

This gives the physical meanings of the triad variables p_b and p_c.[2]

[2]More precisely, in (2.14) p_b and p_c should be $|p_b|$ and $|p_c|$ [12]. With the gauge fixing $p_b > 0$, the opposite sign of p_c corresponds to the inverse spatial orientation, which we do not need to consider in this paper.

B. Classical solution

The vacuum solution of Kantowski-Sachs spacetime is identified with the interior of a Schwarzschild black hole (as will be shown in Sec. II C). The Hamiltonian constraint of the Schwarzschild interior is given in terms of Ashtekar variables as

$$H = -\frac{N}{2G\gamma^2}\left[2bc\sqrt{p_c} + (b^2 + \gamma^2)\frac{p_b}{\sqrt{p_c}}\right]. \tag{2.16}$$

This can be derived from the Hamiltonian constraint of the full theory of LQG. (See [12] or Appendix B of [16].)

To solve the classical solution, we can simplify the Hamiltonian by choosing the lapse function $N = p_b\sqrt{p_c} \equiv \mathbf{V}/4\pi$ and thus introducing the conformal time variable $dt' = (p_b\sqrt{p_c})^{-1}d\tau$. The rescaled Hamiltonian is given by

$$H' = -\frac{1}{2G\gamma^2}[2bcp_bp_c + (b^2 + \gamma^2)p_b^2]. \tag{2.17}$$

The equations of motion are governed by the Hamilton's equations:

$$\frac{dc}{dt'} = \{c, H'\} = 2G\gamma\frac{\partial H'}{\partial p_c} = -2\gamma^{-1}cbp_b, \tag{2.18}$$

$$\frac{dp_c}{dt'} = \{p_c, H'\} = -2G\gamma\frac{\partial H'}{\partial c} = 2\gamma^{-1}p_cbp_b, \tag{2.19}$$

$$\frac{db}{dt'} = \{b, H'\} = G\gamma\frac{\partial H'}{\partial p_b} = -b\gamma^{-1}(bp_b + cp_c) - \gamma p_b, \tag{2.20}$$

$$\frac{dp_b}{dt'} = \{p_b, H'\} = -G\gamma\frac{\partial H'}{\partial b} = \gamma^{-1}p_b(bp_b + cp_c), \tag{2.21}$$

as well as the constraint that the Hamiltonian must vanish:

$$H' = 0 \Rightarrow 2bcp_bp_c + (b^2 + \gamma^2)p_b^2 = 0. \tag{2.22}$$

Notice that substituting (2.14) into (2.19) and (2.21) gives us

$$b = \frac{\gamma}{2\sqrt{p_c}}\frac{dp_c}{d\tau} = \gamma\frac{d}{d\tau}\sqrt{g_{\Omega\Omega}}, \tag{2.23}$$

$$c = \frac{\gamma}{p_c^{1/2}}\frac{dp_b}{d\tau} - \frac{\gamma p_b}{2p_c^{3/2}}\frac{dp_c}{d\tau} = \gamma\frac{d}{d\tau}\left(\frac{p_b}{\sqrt{p_c}}\right) = \gamma\frac{d}{d\tau}(L\sqrt{g_{xx}}), \tag{2.24}$$

which tells that, *classically*, the connection variable b is the time change rate of the square root of the physical area of S^2 [up to constant $(4\pi)^{-1}\gamma$] and c is the time change rate of the physical length of $\mathcal{I}$ (up to constant γ).

To solve the equations of motion, first note that combining (2.18) and (2.19) gives

$$\frac{d}{dt'}(p_c c) = 0 \quad \Rightarrow \quad p_c c = \gamma K_c \text{ is constant}, \tag{2.25}$$

and on the other hand, (2.20) and (2.21) yield

$$\frac{d}{dt'}(K_b) = -p_b^2 \quad \text{with} \quad p_b b =: \gamma K_b(t'). \tag{2.26}$$

The Hamiltonian constraint (2.22) then reads as

$$2K_b K_c + K_b^2 + p_b^2 = 0. \tag{2.27}$$

By (2.26) and (2.27), we have

$$\frac{dK_b}{dt'} = 2K_b K_c + K_b^2, \tag{2.28}$$

the solution of which is given by

$$K_b(t') = -2K_c \frac{\alpha e^{2K_c(t'-t'_0)}}{1+\alpha e^{2K_c(t'-t'_0)}} \tag{2.29}$$

with α being a dimensionless constant specified by the initial state:

$$\alpha := -\frac{K_b(t'_0)}{K_b(t'_0)+2K_c}. \tag{2.30}$$

In terms of $K_b(t')$ and the constant K_c, (2.19) and (2.21) now read as

$$\frac{1}{p_c}\frac{dp_c}{dt'} \equiv \frac{\mathbf{V}}{4\pi p_c}\frac{dp_c}{d\tau} = 2K_b(t'), \tag{2.31}$$

$$\frac{1}{p_b}\frac{dp_b}{dt'} \equiv \frac{\mathbf{V}}{4\pi p_b}\frac{dp_b}{d\tau} = K_b(t') + K_c, \tag{2.32}$$

the solutions to which are given by

$$p_c(t') = g_{\Omega\Omega}(t') = p_c(t'_0)\left(\frac{\alpha+1}{\alpha e^{2K_c(t'-t'_0)}+1}\right)^2 \tag{2.33}$$

and

$$p_b(t') = p_b(t'_0)(\alpha+1)\frac{e^{K_c(t'-t'_0)}}{\alpha e^{2K_c(t'-t'_0)}+1}. \tag{2.34}$$

Consequently, we have

$$g_{xx}(t') = \frac{p_b^2}{L^2 p_c} = \frac{p_b(t'_0)^2}{L^2 p_c(t'_0)} e^{2K_c(t'-t'_0)} \tag{2.35}$$

and

$$\begin{aligned}\mathbf{V}(t') &= 4\pi p_b \sqrt{p_c} \\ &= 4\pi p_b(t'_0)\sqrt{p_c(t'_0)}(\alpha+1)^2 \frac{e^{K_c(t'-t'_0)}}{(\alpha e^{2K_c(t'-t'_0)}+1)^2}.\end{aligned} \tag{2.36}$$

It should be noted that, by (2.31) and (2.32), the time reversal $t' \to -t'$ corresponds to the sign flipping of $K_c \to -K_c$ and $K_b(t') \to -K_b(-t')$ simultaneously. For convenience, we fix the convention $K_c > 0$ for black holes and $K_c < 0$ for white holes. For a black hole, the Hamiltonian constraint (2.27) then yields $K_b(t') < 0$ and consequently $\alpha > 0$.

With the help of (2.27) and (2.30), it can be shown from (2.34) that p_b reaches the maximal value

$$p_{b,\max} = p_b(t'_0)\frac{\alpha+1}{2\sqrt{\alpha}} = K_c \tag{2.37}$$

at the epoch $t' = t'_{\max}$ satisfying $\alpha \exp(2K_c(t'_{\max} - t'_0)) = 1$. That is, the constant $2\pi K_c$ can be interpreted as the maximal value of the area $\mathbf{A}_{x\theta} = \mathbf{A}_{x\phi} \equiv 2\pi p_b$.

The solutions of $K_b(t')$, $p_b(t')$, and $p_c(t)$ all approach to constants asymptotically as $t' \to \pm\infty$. The solutions at the epochs of particular interest are listed as follows:

$$K_b(t') = \begin{cases} -2K_c & \text{as } t' \to \infty, \\ 0 & \text{as } t' \to -\infty, \\ -K_c & \text{as } t' = t'_{\max}, \end{cases} \tag{2.38}$$

$$p_b(t') = \begin{cases} 0 & \text{as } t' \to \pm\infty, \\ p_{b,\max} = K_c & \text{as } t' = t'_{\max}, \end{cases} \tag{2.39}$$

$$p_c(t') = \begin{cases} 0 & \text{as } t' \to \infty, \\ p_c(t'_0)(\alpha+1)^2 \equiv 4G^2M^2 & \text{as } t' \to -\infty, \\ p_c(t'_{\max}) = p_c(t'_0)(\alpha+1)^2/4 \equiv G^2M^2 & \text{as } t' = t'_{\max}. \end{cases} \tag{2.40}$$

Notice that the constant

$$\begin{aligned} p_c(t'_{\max}) = G^2M^2 &\equiv p_c(t'_0)\frac{(\alpha+1)^2}{4} \\ &= p_c(t'_0)\left(\frac{K_c}{K_b(t'_0)+2K_c}\right)^2 \end{aligned} \tag{2.41}$$

$$= p_c(t'_0)\left(\frac{K_b(t'_0)K_c}{p_b(t'_0)^2}\right)^2 \tag{2.42}$$

is independent of t'_0 [this can be shown by taking the derivative of the right-hand side of (2.41) with respect to t'_0 with the help of (2.28) and (2.31)]. In the next section, we will identify the constant $p_c(t'_0)(\alpha+1)^2$ as $4G^2M^2$ with M being the mass of the Schwarzschild black hole (i.e., the area of the horizon is given by $16\pi G^2M^2$).

Additionally, the asymptotic behavior of g_{xx} is given by

$$g_{xx}(t') = \begin{cases} \infty & \text{as } t' \to \infty, \\ 0 & \text{as } t' \to -\infty, \end{cases} \tag{2.43}$$

and that of $\mathbf{V}$ is

$$\mathbf{V}(t') = 0 \quad \text{as } t' \to \pm\infty. \tag{2.44}$$

The behaviors of the classical solution are depicted in Fig. 1. In Sec. II C, we show that the epoch $t' = -\infty$ corresponds to the event horizon of the Schwarzschild

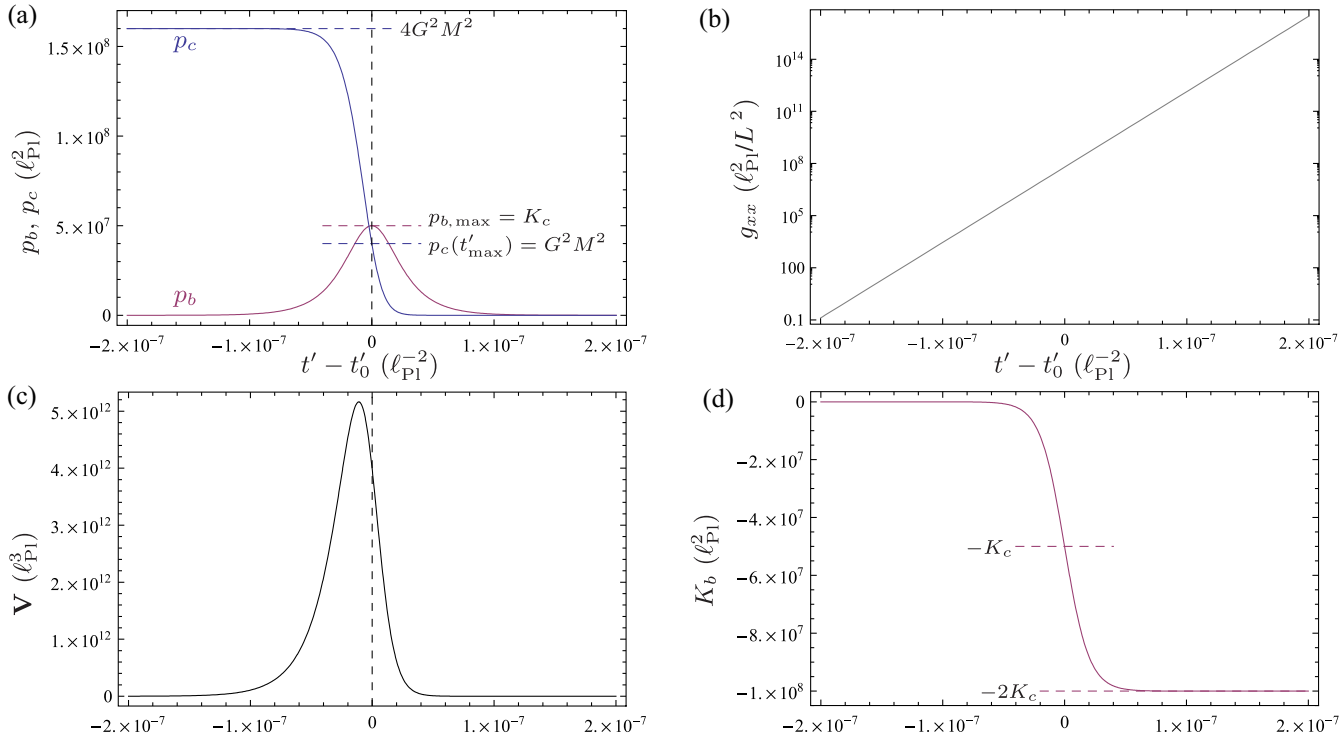

FIG. 1 (color online). Classical solution: The initial condition is given at $t'_0 = t'_{\rm max}$ (and thus $\alpha = 1$) with $p_b(t'_0) = p_{b,\rm max} = K_c = 5. \times 10^7 \ell_{\rm Pl}^2$ and $p_c(t'_0) = p_c(t'_{\rm max}) = G^2M^2 = 4. \times 10^7 \ell_{\rm Pl}^2$ ($\ell_{\rm Pl} := \sqrt{G\hbar}$ is the Planck length). (a) $p_b(t')$ and $p_c(t') = g_{\Omega\Omega}(t')$. (b) $g_{xx}(t')$. (c) $\mathbf{V}(t')$. (d) $K_b(t')$.

black hole and $t' = \infty$ corresponds to the black hole singularity.

Notice that, by (2.14), (2.15), and (2.24), $\mathbf{V}$, p_b, and c depend on the choice of the interval $\mathcal{I}$ and scale as $\mathbf{V}$, p_b, $c \propto L$, while p_c and b are independent of $\mathcal{I}$. As a result, the constants of motion K_c as well as the function $K_b(t')$ both scale as $\propto L$. The ratios $K_c/\mathbf{V}$ and $K_b/\mathbf{V}$ are nevertheless independent of $\mathcal{I}$; hence (2.31) and (2.32) tell that the differential equations for $p_c^{-1}dp_c/d\tau$ and $p_b^{-1}dp_b/d\tau$ in terms of the proper time τ are both independent of $\mathcal{I}$. Therefore, the classical dynamics is *completely independent* of the finite interval $\mathcal{I}$ we choose to make sense of the Hamiltonian formalism. (However, the independence of the choice of $\mathcal{I}$ is not necessarily retained when quantum corrections are taken into account.) Furthermore, the black hole mass M is also independent of $\mathcal{I}$ as can be seen on the right-hand side of (2.41).

There are 4 degrees of freedom in the phase space of p_b, p_c, b, and c. Imposing the Hamiltonian constraint and taking into account the irrelevant choices of the finite interval $\mathcal{I}$ and starting time t'_0, we end up with only $4 - 3 = 1$ genuine degree of freedom. This affirms the "no-hair theorem," which states that, in the case of the vacuum solution without angular momentum, stationary, asymptotically flat black holes are uniquely characterized by one parameter of mass. At the level of phenomenological dynamics with loop quantum corrections, the no-hair theorem remains unchanged for the $\bar{\mu}'$ scheme but requires one extra parameter (due to the dependence on $\mathcal{I}$) in the $\bar{\mu}$ scheme, as will be studied in Sec. III A.

C. Interior of the Schwarzschild black hole

The standard expression of the Schwarzschild metric in terms of spherical coordinates is given by

$$ds^2 = -\left(1 - \frac{2GM}{r}\right)dt^2 + \left(1 - \frac{2GM}{r}\right)^{-1}dr^2 + r^2d\Omega^2, \tag{2.45}$$

which is asymptotically flat (i.e., as $r \to \infty$, the metric components approach those of Minkowski spacetime in spherical coordinates.) Inside the horizon, the temporal and radial coordinates flip roles. To reflect this, we rename the coordinates (r, t) as $(t, \mathcal{L}^{-1}x)$ with an arbitrary scaling factor $\mathcal{L}$. The metric of the Schwarzschild interior now reads as the form of (2.1):

$$\begin{aligned} ds^2 &= -N(t)^2dt^2 + g_{xx}(t)dx^2 + g_{\Omega\Omega}(t)d\Omega^2 \\ &= -\left(\frac{2GM}{t} - 1\right)^{-1}dt^2 + \mathcal{L}^{-2}\left(\frac{2GM}{t} - 1\right)dx^2 \\ &\quad + t^2d\Omega^2, \end{aligned} \tag{2.46}$$

where $t \in [0, 2GM]$, $x \in \mathbb{R}$, and M is the mass of the black hole. The black hole singularity corresponds to $t = 0$ and

the event horizon corresponds to $t = 2GM$. Note that different values of $\mathcal{L}$ correspond to different scalings of x and, thus they all give equivalent metric.[3]

To show that the solution we get in Sec. II B is the Schwarzschild interior, we first identify $g_{\Omega\Omega} = t^2$. The solution in (2.33) then yields

$$e^{2K_c(t'-t'_0)} = \alpha^{-1}\left(-1 + (\alpha+1)\frac{\sqrt{p_c(t'_0)}}{t}\right) \tag{2.47}$$

and

$$-\,p_c(t'_0)\frac{4K_c\alpha(\alpha+1)^2}{(\alpha e^{2K_c(t'-t'_0)}+1)^3}e^{2K_c(t'-t'_0)}dt' = 2tdt. \tag{2.48}$$

Consequently, (2.35) reads as

$$g_{xx} = \frac{4K_c^2}{L^2 p_c(t'_0)(\alpha+1)^2}\left(\frac{(\alpha+1)\sqrt{p_c(t'_0)}}{t} - 1\right) \tag{2.49}$$

and the solutions of (2.33) and (2.34) give

$$d\tau^2 = N(t')^2dt'^2 = \frac{p_b(t'_0)^2}{4K_c^2\alpha p_c(t'_0)}\left(\frac{(\alpha+1)^2 p_c(t'_0)}{\frac{(\alpha+1)\sqrt{p_c(t'_0)}}{t}} - 1\right)dt^2$$

$$= \left(\frac{(\alpha+1)\sqrt{p_c(t'_0)}}{t} - 1\right)^{-1}dt^2 =: N(t)^2dt^2, \tag{2.50}$$

where (2.37) has been used.

If we identify the constant of motion $p_c(t'_{\max})$ in (2.41) as G^2M^2, we then have

$$N^2(t) = \left(\frac{2GM}{t} - 1\right)^{-1} \tag{2.51}$$

and

$$g_{xx}(t) = \left(\frac{K_c}{LGM}\right)^2\left(\frac{2GM}{t} - 1\right), \tag{2.52}$$

which are identical to those in (2.46) with $\mathcal{L} = L(GM/K_c)$.

III. PHENOMENOLOGICAL DYNAMICS WITH LOOP QUANTUM CORRECTIONS

In the fundamental loop quantum theory with Kantowski-Sachs symmetry [12], the Hamiltonian constraint incorporates two main sources of corrections: First, the connection variables b and c do not exist and should be replaced by holonomies; second, the discreteness of quantum geometry also modifies the cotriad component $\omega_c := p_b/\sqrt{p_c} = L\sqrt{g_{xx}}$ such that the eigenvalues of $\hat{\omega}_c$ are finite and significantly different from the classical value near the singularity, at which $p_b/\sqrt{p_c}$ diverges. In the semiclassical description, it is realized that the modification on the cotriad ω_c is less important. At the level of phenomenological analysis, following the procedures adopted for the isotropic cosmology [17] and the Bianchi I model [10], we will ignore the correction on ω_c by simply keeping the classical function $\omega_c = p_b/\sqrt{p_c}$ and take the prescription to replace b, c with

$$b \to \frac{\sin(\bar{\mu}_b b)}{\bar{\mu}_b}, \qquad c \to \frac{\sin(\bar{\mu}_c c)}{\bar{\mu}_c}, \tag{3.1}$$

introducing the variables $\bar{\mu}_b$ and $\bar{\mu}_c$ to impose the fundamental discreteness of loop quantum geometry.[4] The heuristic argument for this prescription can be found in Appendix B of [16] from the perspective of the full (unreduced) theory of LQG.

With the prescription of (3.1) adopted and the cotriad component ω_c unchanged, by choosing $N = \gamma p_b\sqrt{p_c}$ and $dt' = (\gamma p_b\sqrt{p_c})^{-1}d\tau$, the (rescaled) classical Hamiltonian (2.17) is modified to serve as the effective Hamiltonian for the semiclassical theory:

$$H'_{\bar{\mu}} = -\frac{1}{2G\gamma}\left\{2\frac{\sin(\bar{\mu}_b b)}{\bar{\mu}_b}\frac{\sin(\bar{\mu}_c c)}{\bar{\mu}_c}p_b p_c + \left(\frac{\sin(\bar{\mu}_b b)}{\bar{\mu}_b}\right)^2 p_b^2 + \gamma^2 p_b^2\right\}. \tag{3.2}$$

The phenomenological dynamics is then solved as if the dynamics was classical but governed by the new effective Hamiltonian. This treatment is however only heuristic and its validity is still questionable; a more rigorous understanding of the fundamental quantum dynamics would require more sophisticated refinement. Nevertheless, the fact that the phenomenological theory could provide an accurate approximation (for the case where the backreaction is negligible) has been evidenced in the isotropic cosmology [4,17–19] and also affirmed in the Bianchi I models [20].

As for imposing the fundamental discreteness of LQG on the formulation of homogeneous spacetime, the original construction (μ_o scheme) is to take $\bar{\mu}_b$ and $\bar{\mu}_c$ as constants (referred to as μ_b^o, μ_c^o in the Appendix and δ in [12,14,15]). However, it has been shown in both isotropic and Bianchi I models that the μ_o scheme can lead to the wrong semiclassical limit[5] and should be improved by a more sophisticated construction ($\bar{\mu}$ scheme) in which the value of discreteness parameters depends adaptively on the scale factors (e.g., $\bar{\mu} \propto 1/\sqrt{p}$ is used in [4]) and thus

[3] As far as the interior is concerned, $\mathcal{L}$ remains arbitrary. However, if the exterior is also taken into account, there is a canonical convention to fix $\mathcal{L} = 1$ such that $t = \mathcal{L}^{-1}x$ in (2.45) coincides with the proper time in the asymptotically flat regime.

[4] This prescription is sometimes referred to as "polymerization" or "holonomization" in the literature.

[5] For the Schwarzschild interior, due to the absence of matter content, it is not obvious whether the μ_o scheme gives rise to the wrong semiclassical behavior. For completeness, the phenomenological dynamics in the μ_o scheme is presented in the Appendix.

implements the underlying physics of quantum geometry of LQG more directly [4,10].

For the case with Kantowski-Sachs symmetry, there is a variety of possibilities to implement the $\bar{\mu}$-scheme discreteness. Two well-motivated constructions (referred to as the $\bar{\mu}$ scheme and $\bar{\mu}'$ scheme) are focused on in this paper:

(i) $\bar{\mu}$ scheme:

$$\bar{\mu}_b = \sqrt{\frac{\Delta}{p_b}}, \qquad \bar{\mu}_c = \sqrt{\frac{\Delta}{p_c}}, \tag{3.3}$$

(ii) $\bar{\mu}'$ scheme:

$$\bar{\mu}'_b = \sqrt{\frac{\Delta}{p_c}}, \qquad \bar{\mu}'_c = \frac{\sqrt{p_c\Delta}}{p_b}. \tag{3.4}$$

Here Δ is the *area gap* in the full theory of LQG and $\Delta = 2\sqrt{3}\pi\gamma\ell_{\rm Pl}^2$ for the standard choice (but other choices are also possible) with $\ell_{\rm Pl} = \sqrt{G\hbar}$ being the Planck length.

Either scheme has its own merits and until more detailed physics is investigated it remains arguable which one is more sensible. In particular, the $\bar{\mu}$ scheme (in the version for the Bianchi I model) is suggested in [7], since in the construction of the fundamental loop quantum theory the Hamiltonian constraint in the $\bar{\mu}$ scheme gives a difference equation in terms of affine variables and therefore the well-developed framework of the spatially flat and isotropic LQC can be straightforwardly adopted. However, it is argued in [21] that the $\bar{\mu}$ scheme may lead to an unstable difference equation. On the other hand, the $\bar{\mu}'$ scheme does not admit the desirable affine variables but it has the virtue over the $\bar{\mu}$ scheme that its phenomenological dynamics is independent of the choice of $\mathcal{I}$ as will be seen (although this virtue is not necessarily required when quantum corrections are taken into account). To explore their virtues and ramifications, we study both the $\bar{\mu}$ scheme and the $\bar{\mu}'$ scheme at the level of phenomenological dynamics in Secs. III A and III B respectively. (Motivations for both schemes and more comments on them can be found in Appendix B of [16].)

Before going into detail, we can get an idea where the quantum corrections become appreciable by estimating the quantities $\bar{\mu}_b b$, $\bar{\mu}_c c$, etc., which indicate how significant the quantum corrections are (quantum corrections are negligible if $\bar{\mu}_b b$, $\bar{\mu}_c c$, etc. $\ll 1$). Plugging the classical solutions (2.29), (2.33), and (2.34), into (3.3) and (3.4), we have

$$\bar{\mu}_b b = \gamma\bar{\mu}_b\frac{K_b}{p_b} = \gamma\Delta^{1/2}\frac{K_b}{p_b^{3/2}} \to \begin{cases}\infty & \text{as } t'\to\infty,\\ 0 & \text{as } t'\to-\infty,\end{cases} \tag{3.5}$$

$$\bar{\mu}_c c = \gamma\bar{\mu}_c\frac{K_c}{p_c} = \gamma\Delta^{1/2}\frac{K_c}{p_c^{3/2}} \to \begin{cases}\infty & \text{as } t'\to\infty,\\ \frac{\gamma\Delta^{1/2}K_c}{8G^3M^3} & \text{as } t'\to-\infty,\end{cases} \tag{3.6}$$

and

$$\bar{\mu}'_b b = \gamma\bar{\mu}'_b\frac{K_b}{p_b} = 4\pi\gamma\Delta^{1/2}\frac{K_b}{\mathbf{V}} \to \begin{cases}\infty & \text{as } t'\to\infty,\\ 0 & \text{as } t'\to-\infty,\end{cases} \tag{3.7}$$

$$\bar{\mu}'_c c = \gamma\bar{\mu}'_c\frac{K_c}{p_c} = 4\pi\gamma\Delta^{1/2}\frac{K_c}{\mathbf{V}} \to \begin{cases}\infty & \text{as } t'\to\infty,\\ \infty & \text{as } t'\to-\infty.\end{cases} \tag{3.8}$$

Therefore, in the $\bar{\mu}$ scheme, the quantum corrections are significant near the classical singularity and negligible on the horizon provided that

$$K_c \ll \frac{8G^3M^3}{\gamma\sqrt{\Delta}}, \tag{3.9}$$

which can always be satisfied if we choose $\mathcal{I}$ small enough for a given M. On the other hand, in the $\bar{\mu}'$ scheme, both the classical singularity and the horizon receive quantum corrections.

A. Phenomenological dynamics in the $\bar{\mu}$ scheme

The phenomenological dynamics in the $\bar{\mu}$ scheme is specified by the Hamiltonian (3.2) with $\bar{\mu}_b$, $\bar{\mu}_c$ given by (3.3). At the level of phenomenological dynamics, the equations of motion are governed by the Hamilton's equations and the constraint that the Hamiltonian must vanish; these are

$$\begin{aligned}\frac{dc}{dt'} &= \{c, H'_{\bar{\mu}}\} = 2G\gamma\frac{\partial H'_{\bar{\mu}}}{\partial p_c}\\ &= -2\gamma^{-1}\left[\frac{3\sin(\bar{\mu}_c c)}{2\bar{\mu}_c} - \frac{c\cos(\bar{\mu}_c c)}{2}\right]\left[\frac{\sin(\bar{\mu}_b b)}{\bar{\mu}_b}p_b\right],\end{aligned} \tag{3.10}$$

$$\begin{aligned}\frac{dp_c}{dt'} &= \{p_c, H'_{\bar{\mu}}\} = -2G\gamma\frac{\partial H'_{\bar{\mu}}}{\partial c}\\ &= 2\gamma^{-1}p_c\cos(\bar{\mu}_c c)\left[\frac{\sin(\bar{\mu}_b b)}{\bar{\mu}_b}p_b\right],\end{aligned} \tag{3.11}$$

$$\begin{aligned}\frac{db}{dt'} &= \{b, H'_{\bar{\mu}}\} = G\gamma\frac{\partial H'_{\bar{\mu}}}{\partial p_b}\\ &= -\gamma^{-1}\left[\frac{3\sin(\bar{\mu}_b b)}{2\bar{\mu}_b} - \frac{b\cos(\bar{\mu}_b b)}{2}\right]\\ &\quad\times\left[\frac{\sin(\bar{\mu}_b b)}{\bar{\mu}_b}p_b + \frac{\sin(\bar{\mu}_c c)}{\bar{\mu}_c}p_c\right] - \gamma p_b,\end{aligned} \tag{3.12}$$

$$\frac{dp_b}{dt'} = \{p_b, H'_{\bar{\mu}}\} = -G\gamma\frac{\partial H'_{\bar{\mu}}}{\partial b} = \gamma^{-1}p_b\cos(\bar{\mu}_b b)\left[\frac{\sin(\bar{\mu}_b b)}{\bar{\mu}_b}p_b + \frac{\sin(\bar{\mu}_c c)}{\bar{\mu}_c}p_c\right], \tag{3.13}$$

as well as

$$H'_{\bar{\mu}} = 0 \quad \Rightarrow \quad 2\frac{\sin(\bar{\mu}_b b)}{\bar{\mu}_b}\frac{\sin(\bar{\mu}_c c)}{\bar{\mu}_c}p_b p_c + \left[\left(\frac{\sin(\bar{\mu}_b b)}{\bar{\mu}_b}\right)^2 + \gamma^2\right]p_b^2 = 0. \tag{3.14}$$

[Note that in the classical limit $\bar{\mu}_b b,\ \bar{\mu}_c c \to 0$, we have $\sin(\bar{\mu}_b b)/\bar{\mu}_b \to b$, $\sin(\bar{\mu}_c c)/\bar{\mu}_c \to c$ and $\cos(\bar{\mu}_b b)$, $\cos(\bar{\mu}_c c) \to 1$. By inspection, it follows that (3.10), (3.11), (3.12), (3.13), and (3.14) reduce to their classical counterparts (2.18), (2.19), (2.20), (2.21), and (2.22) in the classical limit.] Also notice that (3.11) and (3.13) lead to

$$\frac{\sin(\bar{\mu}_b b)}{\bar{\mu}_b} = \frac{1}{\cos(\bar{\mu}_c c)}\frac{\gamma}{2p_c^{1/2}}\frac{dp_c}{d\tau}, \tag{3.15}$$

$$\frac{\sin(\bar{\mu}_c c)}{\bar{\mu}_c} = \frac{1}{\cos(\bar{\mu}_b b)}\frac{\gamma}{p_c^{1/2}}\frac{dp_b}{d\tau} - \frac{1}{\cos(\bar{\mu}_c c)}\frac{\gamma p_b}{2p_c^{3/2}}\frac{dp_c}{d\tau}, \tag{3.16}$$

which are the modifications of (2.23) and (2.24) with quantum corrections.

Combining (3.10) and (3.11), we have

$$\left[\frac{3\sin(\bar{\mu}_c c)}{2\bar{\mu}_c} - \frac{c\cos(\bar{\mu}_c c)}{2}\right]\frac{dp_c}{dt'} + p_c\cos(\bar{\mu}_c c)\frac{dc}{dt'} = \frac{d}{dt'}\left[p_c\frac{\sin(\bar{\mu}_c c)}{\bar{\mu}_c}\right] = 0, \tag{3.17}$$

which, in accordance with the classical counterpart (2.25), yields the constant of motion:

$$p_c\frac{\sin(\bar{\mu}_c c)}{\bar{\mu}_c} = \gamma K_c. \tag{3.18}$$

Similarly, (3.12) and (3.13) lead to

$$\left[\frac{3\sin(\bar{\mu}_b b)}{2\bar{\mu}_b} - \frac{b\cos(\bar{\mu}_b b)}{2}\right]\frac{dp_b}{dt'} + p_b\cos(\bar{\mu}_b b)\frac{db}{dt'} = \frac{d}{dt'}\left[p_b\frac{\sin(\bar{\mu}_b b)}{\bar{\mu}_b}\right] = -\gamma p_b^2\cos(\bar{\mu}_b b). \tag{3.19}$$

In accordance with the classical counterpart (2.26), we define

$$p_b\frac{\sin(\bar{\mu}_b b)}{\bar{\mu}_b} =: \gamma\bar{K}_b(t'). \tag{3.20}$$

The Hamiltonian constraint (3.14) now reads as

$$2\bar{K}_b K_c + \bar{K}_b^2 + p_b^2 = 0 \tag{3.21}$$

and $\bar{K}_b$ satisfies the differential equation:

$$\frac{d\bar{K}_b}{dt'} = \cos(\bar{\mu}_b b)(2\bar{K}_b K_c + \bar{K}_b^2). \tag{3.22}$$

Substituting (3.18) and (3.20) into (3.11) and (3.13) yields

$$\frac{1}{p_c}\frac{dp_c}{dt'} \equiv \frac{\mathbf{V}}{4\pi p_c}\frac{dp_c}{d\tau} = 2\cos(\bar{\mu}_c c)\bar{K}_b, \tag{3.23}$$

$$\frac{1}{p_b}\frac{dp_b}{dt'} \equiv \frac{\mathbf{V}}{4\pi p_b}\frac{dp_b}{d\tau} = \cos(\bar{\mu}_b b)[\bar{K}_b + K_c]. \tag{3.24}$$

Note that, as in the classical dynamics, it follows from (3.22) that the flipping $K_c \to -K_c$ gives rise to $\bar{K}_b(t') \to -\bar{K}_b(-t')$ and thus corresponds to the time reversal according to (3.23) and (3.24).

Equations (3.23) and (3.24) are the modifications of their classical counterparts (2.31) and (2.32). Notice that the presence of the $\cos(\cdots)$ terms gives rise to the *repulsive* behavior of gravity as the evolution departs from the classical solution. More precisely, in the $\bar{\mu}$-scheme phenomenological dynamics, p_c and p_b get bounced whenever $\cos(\bar{\mu}_c c)$ or $\cos(\bar{\mu}_b b)$ flips signs, respectively. To find out the exact moment of occurrence of the bounces, we investigate $\cos(\bar{\mu}_c c)$ and $\cos(\bar{\mu}_b b)$ in more detail.

By (3.18) and (3.20), we have

$$\cos(\bar{\mu}_c c) = \pm[1 - \sin^2\bar{\mu}_c c]^{1/2} = \pm\left[1 - \frac{\gamma^2 K_c^2\Delta}{p_c^3}\right]^{1/2}, \tag{3.25}$$

$$\cos(\bar{\mu}_b b) = \pm[1 - \sin^2\bar{\mu}_b b]^{1/2} = \pm\left[1 - \frac{\gamma^2\bar{K}_b^2\Delta}{p_b^3}\right]^{1/2}. \tag{3.26}$$

Consequently, p_c and p_b get bounced, as $\cos(\bar{\mu}_c c)$ flips signs in (3.23) and $\cos(\bar{\mu}_b b)$ flips signs in (3.24) respectively, whenever

$$p_c = (\gamma^2 K_c^2\Delta)^{1/3} \ll 4G^2M^2, \tag{3.27}$$

$$p_b = (\gamma^2\bar{K}_b^2\Delta)^{1/3} \approx (4\gamma^2 K_c^2\Delta)^{1/3} \ll 4^{4/3}G^2M^2, \tag{3.28}$$

where we have used (3.9) and exploited the fact that $K_b \to -2K_c$ as the classical solution is close to the singularity.

To sum up, the classical black hole singularity is replaced by the quantum bounce, which makes both p_c and p_b bounced at the (different) epochs when the conditions (3.27) and (3.28) are met, respectively. [Furthermore, with the $\cos(\bar{\mu}_b b)$ term in (3.22), $\bar{K}_b$ becomes flat ($d\bar{K}_b/dt' = 0$) exactly at the same time when p_b gets bounced.] Across the quantum bounce, the evolution tends to be classical again [as $\cos(\bar{\mu}_b b)$, $\cos(\bar{\mu}_c c) \to -1$ eventually]; as a result, the classical solution is connected with another classical solution through the quantum bounce.

Notice that the constant K_c remains the same throughout the evolution. However, this does not mean that the parameter used to parametrize the classical evolutions on both sides of the bounce remains unchanged, since the physical meanings of $p_b b$ and $p_c c$ are changed before and after the bounce according to (3.15) and (3.16). In order to characterize the classical behaviors of the evolution in different classical periods, we define the "effective K_c" as

$$\begin{aligned}\text{effective } K_c &:= \gamma^{-1} p_c \left(\frac{\gamma}{p_c^{1/2}} \frac{dp_b}{d\tau} - \frac{\gamma p_b}{2p_c^{3/2}} \frac{dp_c}{d\tau}\right) \\ &= \gamma^{-1} \cos(\bar{\mu}_b b) p_c \frac{\sin(\bar{\mu}_c c)}{\bar{\mu}_c} \\ &\quad + \gamma^{-1}[\cos(\bar{\mu}_b b) \\ &\quad - \cos(\bar{\mu}_c c)] p_b \frac{\sin(\bar{\mu}_b b)}{\bar{\mu}_b} \\ &= \cos(\bar{\mu}_b b) K_c + [\cos(\bar{\mu}_b b) - \cos(\bar{\mu}_c c)] \bar{K}_b \end{aligned} \tag{3.29}$$

and similarly the "effective K_b" as

$$\begin{aligned}\text{effective } K_b &:= \gamma^{-1} p_b \left(\frac{\gamma}{2p_c^{1/2}} \frac{dp_c}{d\tau}\right) \\ &= \gamma^{-1} \cos(\bar{\mu}_c c) p_b \frac{\sin(\bar{\mu}_b b)}{\bar{\mu}_b} \\ &= \cos(\bar{\mu}_c c) \bar{K}_b. \end{aligned} \tag{3.30}$$

In the classical regimes, $\cos(\bar{\mu}_b b) \approx \cos(\bar{\mu}_c c) \approx \pm 1$ and we have

$$\text{effective } K_c \approx \pm K_c, \tag{3.31}$$

$$\text{effective } K_b \approx \pm K_b. \tag{3.32}$$

That is, on the other side of the bounce, both (classical) K_c and K_b flip signs and consequently the quantum bounce bridges the interior of a classical black hole with that of a classical white hole and vice versa.

To know the mass of the white hole, in accordance with (2.42), we define the "effective mass" as

$$\text{effective mass} := G^{-1} \frac{\sqrt{p_c}}{p_b} |\text{effective } K_c||\text{effective } K_b|. \tag{3.33}$$

Note that effective K_b approaches $\mp 2K_c$ right before and after the bounce, leaving the factor $|\text{effective } K_b||\text{effective } K_c|$ unchanged; however, the ratio $\sqrt{p_c}/p_b$ is not fixed and thus (3.33) yields unequal masses before and after the quantum bounce. Therefore, for a given black hole mass M, generally, the mass of the conjoined white hole (denoted as M') is different from M. The exact value of M' depends on the detail of the initial condition, which involves the choice of $\mathcal{I}$.

It is noteworthy that, in contrast to the classical dynamics, the phenomenological dynamics in the $\bar{\mu}$ scheme is *dependent* on the choice of the finite sized interval $\mathcal{I}$. In particular, M' depends on $\mathcal{I}$; moreover, (3.27) and (3.28), which indicate occurrence of the bounce, are not invariant under rescaling of $\mathcal{I}$ (recall $p_b \propto L$, $p_c \propto L^0$, and $K_c \propto L$). For this matter, one might think that the $\bar{\mu}$-scheme quantization is simply ill defined and should be discarded. However, it would be premature to dismiss the $\bar{\mu}$ scheme immediately as it is a common phenomenon that a quantum system reacts to macroscopic scales introduced by boundary conditions (for instance, the well-known "conformal anomaly" as a "soft" breaking of conformal symmetry). From the perspective of the full theory of LQG, the inhomogeneous degrees of freedom, which have been ignored in the symmetry-reduced minisuperspace formulation, could give rise to a macroscopic scale and thus account for the dependence on $\mathcal{I}$. (In the lattice refining model of [21], this is indeed the case that, depending on the details of the refining procedure, the characteristic size of the lattice may leave imprints on the coarse-grained homogeneous description.) This suggests that the choice of $\mathcal{I}$ is not merely a gauge fixing but reflects the underlying physics of quantum inhomogeneity and thus has a physical consequence. In the language of the no-hair theorem, this physical consequence dictates that one extra parameter M' (or equivalently, say K_c) is needed to completely characterize the extended Schwarzschild black hole, even though the information of M' is hidden by the horizon and inaccessible (at least semiclassically) to the external observer (cf. the apparent problem of dependence on $\mathcal{I}$ is absent in the phenomenological dynamics of the $\bar{\mu}$ scheme as will be seen in Sec. III B).

For given initial conditions, the equations of motion can be solved numerically.[6] The numerical solution is depicted in Fig. 2. Note that the bounces of p_c and p_b occur at the moments exactly as indicated in (3.27) and (3.28). Also notice that p_b is perfectly symmetric about the bounce, since (3.22) and (3.24) are independent of p_c and c and, as a result, the evolution of p_b is unaffected by the varying of p_c (but not vice versa).

B. Phenomenological dynamics in the $\bar{\mu}'$ scheme

The phenomenological dynamics in the $\bar{\mu}'$ scheme is specified by the effective Hamiltonian (3.2) with $\bar{\mu}_b$, $\bar{\mu}_c$ replaced by $\bar{\mu}'_b$, $\bar{\mu}'_c$ given in (3.4). To simplify the equations of motion, we choose a different lapse function $N =$

[6]The common numerical methods (e.g., the Runge-Kutta method) encounter numerical instability at some point if we directly solve the coupled differential equations (3.10), (3.11), (3.12), and (3.13). To bypass this problem, which is only a numerical artifact, we solve the reduced coupled equations: (3.22), (3.23), and (3.24) for three variables: $\bar{K}_b$, p_c, and p_b. The variables b and c can be obtained afterward via (3.18) and (3.20).

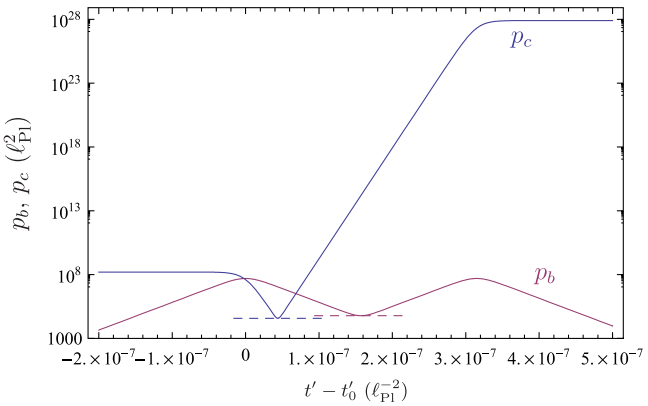

FIG. 2 (color online). Solution in the $\bar{\mu}$-scheme phenomenological dynamics: With the same initial condition as given in Fig. 1 and the Barbero-Immirzi parameter is set to $\gamma = \ln 2/(\sqrt{3}\pi)$. The conditions of (3.27) and (3.28) are indicated by dashed lines, at which p_c and p_b get bounced, respectively. The quantum bounce bridges the classical black hole (on the left side) with the classical white hole (on the right side). The asymptotic values of p_c are different on both sides, indicating that the black hole mass M and white hole mass M' are different. On the other hand, p_b is symmetric and, in particular, the peaks on both sides are of the same height, affirming that K_c flips signs but its magnitude is unchanged as suggested in (3.31).

$(p_b\sqrt{p_c})^{-1}$ associated with the new time variable $dt'' = p_b\sqrt{p_c}d\tau$. With the new lapse, the Hamiltonian (3.2) is further rescaled to the simpler form:

$$H''_{\bar{\mu}'} = -\frac{1}{2G\gamma^2\Delta}\Big\{2\sin(\bar{\mu}'_b b)\sin(\bar{\mu}'_c c) + \sin^2(\bar{\mu}_b b) + \Delta\frac{\gamma^2}{p_c}\Big\}. \tag{3.34}$$

Because $|\sin(\bar{\mu}'_I c_I)| \le 1$, the vanishing of the Hamiltonian constraint $H''_{\bar{\mu}'} = 0$ immediately implies

$$|p_c| = \frac{\gamma^2\Delta}{|2\sin(\bar{\mu}'_b b)\sin(\bar{\mu}'_c c) + \sin^2(\bar{\mu}_b b)|} \ge \frac{\gamma^2}{3}\Delta. \tag{3.35}$$

This suggests that p_c is bounded below.

To know the detailed dynamics for each individual p_b and p_c, in addition to the Hamiltonian constraint, we study the Hamilton's equations:

$$\frac{dc}{dt''} = \{c, H''_{\bar{\mu}'}\} = 2G\gamma\frac{\partial H''_{\bar{\mu}'}}{\partial p_c} = -\frac{c\bar{\mu}'_c\cos(\bar{\mu}'_c c)\sin(\bar{\mu}'_b b)}{\gamma\Delta p_c} + \frac{b\bar{\mu}'_b\cos(\bar{\mu}'_b b)[\sin(\bar{\mu}'_b b) + \sin(\bar{\mu}'_c c)]}{\gamma\Delta p_c} + \frac{\gamma}{p_c^2}, \tag{3.36}$$

$$\frac{dp_c}{dt''} = \{p_c, H''_{\bar{\mu}'}\} = -2G\gamma\frac{\partial H''_{\bar{\mu}'}}{\partial c} = \frac{2\bar{\mu}'_c\cos(\bar{\mu}'_c c)\sin(\bar{\mu}'_b b)}{\gamma\Delta}, \tag{3.37}$$

$$\frac{db}{dt''} = \{b, H''_{\bar{\mu}'}\} = G\gamma\frac{\partial H''_{\bar{\mu}'}}{\partial p_b} = \frac{c\bar{\mu}'_c\cos(\bar{\mu}'_c c)\sin(\bar{\mu}'_b b)}{\gamma\Delta p_b}, \tag{3.38}$$

$$\frac{dp_b}{dt''} = \{p_b, H''_{\bar{\mu}'}\} = -G\gamma\frac{\partial H''_{\bar{\mu}'}}{\partial b} = \frac{\bar{\mu}'_b\cos(\bar{\mu}'_b b)[\sin(\bar{\mu}'_b b) + \sin(\bar{\mu}'_c c)]}{\gamma\Delta}. \tag{3.39}$$

Note that (3.37) and (3.39) give us

$$\frac{\sin(\bar{\mu}'_b b)}{\bar{\mu}'_b} = \frac{1}{\cos(\bar{\mu}'_c c)}\frac{\gamma}{2p_c^{1/2}}\frac{dp_c}{d\tau}, \tag{3.40}$$

$$\frac{\sin(\bar{\mu}'_c c)}{\bar{\mu}'_c} = \frac{1}{\cos(\bar{\mu}'_b b)}\frac{\gamma}{p_c^{1/2}}\frac{dp_b}{d\tau} - \frac{1}{\cos(\bar{\mu}'_c c)}\frac{\gamma p_b}{2p_c^{3/2}}\frac{dp_c}{d\tau}, \tag{3.41}$$

which are the modifications of (2.23) and (2.24) with quantum corrections.

Inspecting (3.36), (3.37), (3.38), and (3.39), we have

$$\frac{d}{dt''}(p_c c - p_b b) = \frac{\gamma}{p_c}. \tag{3.42}$$

In accordance with the constant K_c and the function $K_b(t')$ used for classical solutions in (2.25) and (2.26), introducing the time-varying function $f(t'')$, we set

$$p_c c = \gamma(K_c + f(t'')) \tag{3.43}$$

and

$$p_b b =: \gamma(\bar{K}'_b(t'') + f(t'')), \tag{3.44}$$

where $\bar{K}'_b$ satisfies

$$p_b^2 p_c\frac{d\bar{K}'_b}{dt''} = \frac{d\bar{K}'_b}{dt'} = -p_b^2, \tag{3.45}$$

which is to be compared with the classical counterpart (2.26). Starting in a classical regime, we set $K_c \approx \gamma^{-1}p_c c$ and $f \approx 0$.

Substituting (3.43) and (3.44) into (3.34), we have the complicated expression for the Hamiltonian constraint $H''_{\bar{\mu}'} = 0$:

$$2\sin\left(\sqrt{\frac{\Delta\gamma^2}{p_b^2 p_c}}(\bar{K}_b' + f)\right)\sin\left(\sqrt{\frac{\Delta\gamma^2}{p_b^2 p_c}}(K_c + f)\right) + \sin^2\left(\sqrt{\frac{\Delta\gamma^2}{p_b^2 p_c}}(\bar{K}_b' + f)\right) = -\frac{\Delta\gamma^2}{p_c}, \tag{3.46}$$

which reduces to

$$2\bar{K}_b' K_c + \bar{K}_b'^2 + p_b^2 = 0 \tag{3.47}$$

in the classical limit as $p_b^2 p_c \gg \Delta\gamma^2 K_\phi^2 \sim \Delta\gamma^2 K_c^2 \sim \Delta\gamma^2 K_{b,\pm}^2$ and with $f \approx 0$.

As discussed earlier, in the $\bar{\mu}$ scheme, the quantum corrections take effect both near the classical singularity and the event horizon. Thus, it is expected that the classical singularity is resolved and replaced by the late time quantum bounce and the event horizon is diffused by the early time quantum bounce. Across the quantum bounces, we would guess, the evolution becomes classical again; as a result, the late/early time quantum bounce bridges one cycle of classical evolution with the next/previous classical cycle.

As in the $\bar{\mu}$ scheme, the constant K_c remains fixed throughout the evolution but since $p_b b$ and $p_c c$ have different physical meanings before and after the quantum bounce according to (3.40) and (3.41), analogous to (3.29), (3.30), and (3.33), we define

$$\begin{aligned}\text{effective } K_c &:= \gamma^{-1} p_c\left(\frac{\gamma}{p_c^{1/2}}\frac{dp_b}{d\tau} - \frac{\gamma p_b}{2p_c^{3/2}}\frac{dp_c}{d\tau}\right)\\ &= \gamma^{-1}\cos(\bar{\mu}_b' b)p_c\frac{\sin(\bar{\mu}_c' c)}{\bar{\mu}_c'} + \gamma^{-1}[\cos(\bar{\mu}_b' b) - \cos(\bar{\mu}_c' c)]p_b\frac{\sin(\bar{\mu}_b' b)}{\bar{\mu}_b'},\end{aligned} \tag{3.48}$$

$$\begin{aligned}\text{effective } K_b &:= \gamma^{-1} p_b\left(\frac{\gamma}{2p_c^{1/2}}\frac{dp_c}{d\tau}\right)\\ &= \gamma^{-1}\cos(\bar{\mu}_c' c)p_b\frac{\sin(\bar{\mu}_b' b)}{\bar{\mu}_b'}\end{aligned} \tag{3.49}$$

and

$$\text{effective mass} := G^{-1}\frac{\sqrt{p_c}}{p_b}|\text{effective } K_c||\text{effective } K_b| \tag{3.50}$$

to characterize the classical evolution in different classical periods.

Starting with $f \approx 0$ and $p_c c \approx \gamma K_c$ in a given cycle of classical phase, we would guess f varies widely when it undergoes the bounce but anchors to a nonzero constant (such that effective $K_c \approx K_c + f$) in the consecutive classical cycle when it jumps over the bounce. (The numerical analysis shows that this indeed is the case.) At the epoch right before the late time bounce, we have effective $K_c \approx K_c$, effective $K_b \approx K_b \approx -2K_c$, and $p_b \approx 0$; immediately after the late time bounce, we then have effective $K_c \approx K_c + f$, effective $K_b \approx -2K_c + f$, and $p_b \approx 0$, which should satisfy the classical Hamiltonian constraint (2.27) and thus give

$$2(-2K_c + f)(K_c + f) + (-2K_c + f)^2 \approx 0. \tag{3.51}$$

This yields $f \approx 0$ or $f \approx 2K_c$ and consequently implies that the effective K_c is altered to be $K_c + f \approx 3K_c$ and effective $K_b \approx K_b + f \approx 0$ right after the late time bounce. Similarly, starting with effective $K_c \approx K_c$, effective $K_b \approx K_b \approx 0$, and $p_b \approx 0$ at the epoch close to the early time bounce, we can infer that $f \approx -2K_c/3$, effective $K_c \approx K_c + f \approx K_c/3$, and effective $K_b \approx K_b + f \approx -2K_c/3$ immediately across the early time bounce. We then conclude that the quantum bounce resolves the black hole singularity and bridges it with the diffused horizon of another black hole (not white hole); the parameter K_c in one cycle of classical phase is shifted to $3K_c$ in the next classical cycle and to $K_c/3$ in the previous cycle. Schematically, the varying of the effective K_c is summarized as

$$\cdots \frac{K_c}{3^2} \overset{\text{bounce}}{\longleftrightarrow} \frac{K_c}{3} \overset{\text{bounce}}{\longleftrightarrow} K_c \overset{\text{bounce}}{\longleftrightarrow} 3K_c \overset{\text{bounce}}{\longleftrightarrow} 3^2 K_c \cdots. \tag{3.52}$$

To find out the precise condition for the occurrence of quantum bounces, by substituting (3.43) and (3.44) into (3.37) and (3.39), we study the differential equations:

$$\begin{aligned}\frac{1}{p_c}\frac{dp_c}{dt'} &\equiv \frac{\mathbf{V}}{4\pi p_c}\frac{dp_c}{d\tau}\\ &= 2\sqrt{\frac{p_b^2 p_c}{\gamma^2\Delta}}\cos\left(\sqrt{\frac{\gamma^2\Delta}{p_b^2 p_c}}(K_c + f)\right)\times\sin\left(\sqrt{\frac{\gamma^2\Delta}{p_b^2 p_c}}(\bar{K}_b' + f)\right),\end{aligned} \tag{3.53}$$

$$\begin{aligned}\frac{1}{p_b}\frac{dp_b}{dt'} &\equiv \frac{\mathbf{V}}{4\pi p_b}\frac{dp_b}{d\tau}\\ &= \sqrt{\frac{p_b^2 p_c}{\gamma^2\Delta}}\cos\left(\sqrt{\frac{\gamma^2\Delta}{p_b^2 p_c}}(\bar{K}_b' + f)\right)\times\left[\sin\left(\sqrt{\frac{\gamma^2\Delta}{p_b^2 p_c}}(\bar{K}_b' + f)\right) + \sin\left(\sqrt{\frac{\gamma^2\Delta}{p_b^2 p_c}}(K_c + f)\right)\right].\end{aligned} \tag{3.54}$$

These are the modifications of the classical counterparts (2.31) and (2.32).

Similar to the case of (3.23) in the $\bar{\mu}$ scheme, p_c gets bounced once the "cos(···)" term in (3.53) flips signs.[7] This happens when

$$\cos\left(\sqrt{\frac{\gamma^2\Delta}{p_b^2 p_c}}(K_c+f)\right)=0\Rightarrow K_c+f=\frac{\pi}{2}\sqrt{\frac{p_b^2 p_c}{\gamma^2\Delta}}. \tag{3.55}$$

Assuming p_b also gets bounced roughly around the same moment,[8] at which (3.55) is satisfied, we have the approximation:

$$\begin{aligned}\sin\left(\sqrt{\frac{\gamma^2\Delta}{p_b^2 p_c}}(\bar{K}_b'+f)\right)&=\sin\left(\frac{\pi}{2}+\sqrt{\frac{\gamma^2\Delta}{p_b^2 p_c}}(\bar{K}_b'-K_c)\right)\\&=\cos\left(\sqrt{\frac{\gamma^2\Delta}{p_b^2 p_c}}(\bar{K}_b'-K_c)\right)\\&\approx 1-\frac{1}{2!}\frac{\gamma^2\Delta}{p_b^2 p_c}(\bar{K}_b'-K_c)^2+\frac{1}{4!}\\&\quad\times\left(\frac{\gamma^2\Delta}{p_b^2 p_c}\right)^2(\bar{K}_b'-K_c)^4+\cdots.\end{aligned} \tag{3.56}$$

Taking (3.55) and (3.56) into (3.46), we have

$$\begin{aligned}0\approx 2\frac{p_b^2 p_c}{\gamma^2\Delta}\Bigg[&1-\frac{\gamma^2\Delta}{2p_b^2 p_c}(\bar{K}_b'-K_c)^2+\frac{1}{4!}\left(\frac{\gamma^2\Delta}{p_b^2 p_c}\right)^2\\&\times(\bar{K}_b'-K_c)^4\Bigg]+\frac{p_b^2 p_c}{\gamma^2\Delta}\Bigg[1-\frac{\gamma^2\Delta}{2p_b^2 p_c}(\bar{K}_b'-K_c)^2\\&+\frac{1}{4!}\left(\frac{\gamma^2\Delta}{p_b^2 p_c}\right)^2(\bar{K}_b'-K_c)^4\Bigg]^2+p_b^2+\cdots,\end{aligned} \tag{3.57}$$

which, provided that $p_b,\ p_c\gg\gamma^2\Delta$ when the bounce occurs,[9] leads to the condition for occurrence of the bounce in p_c:

$$\begin{aligned}\frac{\gamma^2\Delta}{p_b^2 p_c}&\approx\frac{2(3-\sqrt{3})}{(\bar{K}_b'-K_c)^2}\\&\approx\begin{cases}\frac{2(3-\sqrt{3})}{9K_c^2} & \text{for the late time bounce in } p_c,\\ \frac{2(3-\sqrt{3})}{K_c^2} & \text{for the early time bounce in } p_c.\end{cases}\end{aligned} \tag{3.58}$$

Here, we have exploited the fact that (2.28) and (3.45) are formally identical and therefore $\bar{K}_b'$ remains almost constant ($\bar{K}_b'\approx K_b\to -2K_c$ or 0) close to the late/early time bounce even when quantum corrections take effect later. (In the bouncing period, the quantum effect varies f dramatically but modifies $\bar{K}_b'$ only slightly.)[10]

Similarly, p_b gets bounced once the cos(···) term in (3.54) flips signs. Following the same argument above, we conclude that the big bounce of p_b happens when

$$\begin{aligned}0\approx 2\frac{p_b^2 p_c}{\gamma^2\Delta}\Bigg[&1-\frac{\gamma^2\Delta}{2p_b^2 p_c}(\bar{K}_b'-K_c)^2+\frac{1}{4!}\left(\frac{\gamma^2\Delta}{p_b^2 p_c}\right)^2\\&\times(\bar{K}_b'-K_c)^4\Bigg]+\frac{p_b^2 p_c}{\gamma^2\Delta}+p_b^2+\cdots,\end{aligned} \tag{3.59}$$

which leads to the condition for occurrence of the bounce in p_b:

$$\begin{aligned}\frac{\gamma^2\Delta}{p_b^2 p_c}&\approx\frac{6}{(\bar{K}_b'-K_c)^2}\\&\approx\begin{cases}\frac{2}{3K_c^2} & \text{for the late time bounce in } p_b,\\ \frac{6}{K_c^2} & \text{for the early time bounce in } p_b.\end{cases}\end{aligned} \tag{3.60}$$

Since the Taylor series of $\cos x=1-x^2/2+x^4/4!+\cdots$ converges very rapidly, the approximation made above is fairly accurate if

$$|x|=\sqrt{\frac{\gamma^2\Delta}{p_b^2 p_c}}|\bar{K}_b'-K_c|<\pi, \tag{3.61}$$

which is satisfied for both (3.58) and (3.60).

Knowing the conditions for occurrence of bounces, we are able to estimate the black hole mass in different classical cycles. Let M be the mass of a given classical cycle with the constant K_c; (2.42) then tells us

$$G^2M^2=p_c(\check{t}_-'')\left(\frac{K_b(\check{t}_-'')K_c}{p_b(\check{t}_-'')^2}\right)^2\approx 4\frac{p_c(\check{t}_-'')}{p_b(\check{t}_-'')^4}K_c^4, \tag{3.62}$$

where we denote the epoch of the late time bounce in p_c as $\check{t}''$ and the instant right before $\check{t}''$ as $\check{t}_-''$, at which the quantum effect is still negligible and the evolution is classical enough so that $K_b(\check{t}_-'')\to -2K_c$. On the other hand, let $\mathfrak{M}$ be the mass of the black hole in the next classical cycle after the big bounce; (2.41) then gives us

[7]The numerical result further shows that once the cos(···) term in (3.23) or (3.24) flips signs from +1 to −1, it quickly flips back to +1. Both $\cos(\bar{\mu}_c'c)$ and $\cos(\bar{\mu}_b'b)$ flip *twice* during the bouncing period. This concurs with the previous finding that the quantum bounce bridges the black hole with another black hole (instead of a white hole). By contrast, in the $\bar{\mu}$ scheme, $\cos(\bar{\mu}_c c)$ and $\cos(\bar{\mu}_c c)$ flip from +1 to −1 only once and thus the quantum bounce conjoins a black hole with a white hole.

[8]This is because (3.53) and (3.54) are coupled through $\mathbf{V}=4\pi p_b\sqrt{p_c}$. We can see that this is indeed the case in the numerical solution.

[9]We will see that this is true until p_c eventually descends into the deep Planck regime in the far late time.

[10]Do not confuse $\bar{K}_b'$ with effective K_b. The former remains constant through the bounce while the latter is offset by f.

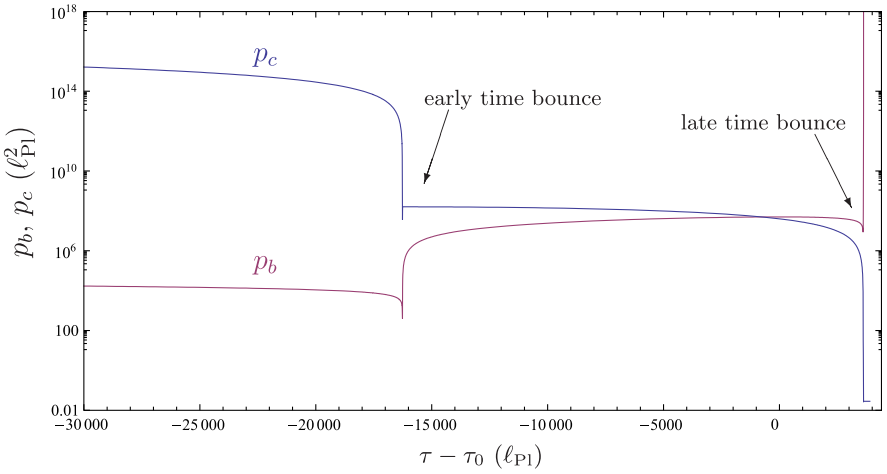

FIG. 3 (color online). Solution in the $\bar{\mu}'$-scheme phenomenological dynamics: With the same initial condition as given in Fig. 1 and the Barbero-Immirzi parameter is set to $\gamma = \ln 2/(\sqrt{3}\pi)$. τ is the proper time and $\tau_0 = \tau(t_0')$. The event horizon is diffused by the early time bounce and connected to another black hole of a larger mass. The classical singularity is resolved and replaced by the late time bounce, which bridges the black hole with another black hole of a smaller mass. The vicinity of the early time bounce is zoomed in in Fig. 4 and that of the late time bounce in Fig. 5.

$$G^2\mathfrak{M}^2 = p_c(\check{t}_+'')\left(\frac{K_c}{K_b(\check{t}_+'') + 2K_c}\right)^2 \approx \frac{p_c(\check{t}_+'')}{4}, \tag{3.63}$$

where we denote the instant right after $\check{t}''$ as $\check{t}_+''$, at which the evolution is classical enough and thus $K_b(\check{t}_+'') \to 0$. Meanwhile, at $\check{t}''$, (3.58) also tells us

$$\frac{\gamma^2\Delta}{p_b(\check{t}'')^2 p_c(\check{t}'')} \approx \frac{2(3-\sqrt{3})}{9K_c^2}. \tag{3.64}$$

Assuming that $\check{t}$, $\check{t}_+$, and $\check{t}_-$ are fairly close to one another so that $p_c(\check{t}_+) \approx p_c(\check{t}_-) \approx p_c(\check{t})$ and $p_b(\check{t}) \approx p_b(\check{t}_-)$, we can infer from (3.62), (3.63), and (3.64) that

$$\begin{aligned}\mathfrak{M}(M) &\approx \left(\frac{9}{32(3-\sqrt{3})}\right)^{1/3}\left(\frac{\gamma^2\Delta M}{G^2}\right)^{1/3} \\ &\simeq 0.605\left(\frac{\gamma^2\Delta M}{G^2}\right)^{1/3}.\end{aligned} \tag{3.65}$$

While this analysis gives a very good estimate with small error due to approximation, the detailed numerical solution gives the more precise result

$$\mathfrak{M}(M) \simeq 0.524\left(\frac{\gamma^2\Delta M}{G^2}\right)^{1/3} \simeq 1.161(m_{\rm Pl}^2 M)^{1/3}, \tag{3.66}$$

where $m_{\rm Pl} := \sqrt{\hbar/G}$ is the Planck mass. As a result, the *effective mass* is tremendously decreased by the late time bounces until it eventually approaches $\sim m_{\rm Pl}$; schematically, the varying of the effective mass is summarized as

$$\begin{aligned}\cdots\mathfrak{M}^{-1}(\mathfrak{M}^{-1}(M)) &\overset{\text{bounce}}{\longleftrightarrow}\mathfrak{M}^{-1}(M)\overset{\text{bounce}}{\longleftrightarrow}M\overset{\text{bounce}}{\longleftrightarrow}\mathfrak{M}(M) \\ &\overset{\text{bounce}}{\longleftrightarrow}\mathfrak{M}(\mathfrak{M}(M))\cdots.\end{aligned} \tag{3.67}$$

The differential equations (3.36), (3.37), (3.38), and (3.39) can be solved numerically for a given initial condition. The numerical solution is shown in Fig. 3, which depicts both the late time and the early time quantum bounces. The vicinity of the early time bounce is zoomed in in Fig. 4 and that of the late time bounce in Fig. 5. The early/late time quantum bounce bridges a classical phase with another classical phase in the previous/next cycle. Contrary to the $\bar{\mu}$ scheme, the epochs of bounces in p_c and p_b are very close to each other (see footnote 8). Toward the future, the effective K_c becomes larger and larger while the effective mass becomes smaller and smaller. As can be seen in Fig. 5, the semiclassicality is less and less established and eventually p_b grows exponentially (with respect to τ) while p_c asymptotically descends to a constant in the deep Planck regime, in which the quantum fluctuations become essential.

Although the validity of the semiclassical analysis might break down when the solution descends into the deep Planck regime,[11] it is still instructive to know the asymptotic behavior within the same phenomenological framework. To find out the asymptotic solution, we assume $p_c = \bar{p}_c$, $p_b = \bar{p}_b e^{\kappa\tau}$ with constants $\bar{p}_c$, $\bar{p}_b$, and κ. By (3.37) and (3.39), we have

$$\frac{1}{p_c}\frac{dp_c}{d\tau} = 0 = \frac{2}{\gamma\sqrt{\Delta}}\cos(\bar{\mu}_c' c)\sin(\bar{\mu}_b' b), \tag{3.68}$$

$$\frac{1}{p_b}\frac{dp_b}{d\tau} = \kappa = \frac{1}{\gamma\sqrt{\Delta}}\cos(\bar{\mu}_b' b)[\sin(\bar{\mu}_b' b) + \sin(\bar{\mu}_c' c)], \tag{3.69}$$

which yield $\bar{\mu}_c' c = (2n + 1/2)\pi$ with $n \in \mathbb{Z}$ [such that

[11] In particular, the cotriad component $\omega_c = L\sqrt{g_{xx}}$ grows exponentially and the quantum corrections on it have to be taken into account.

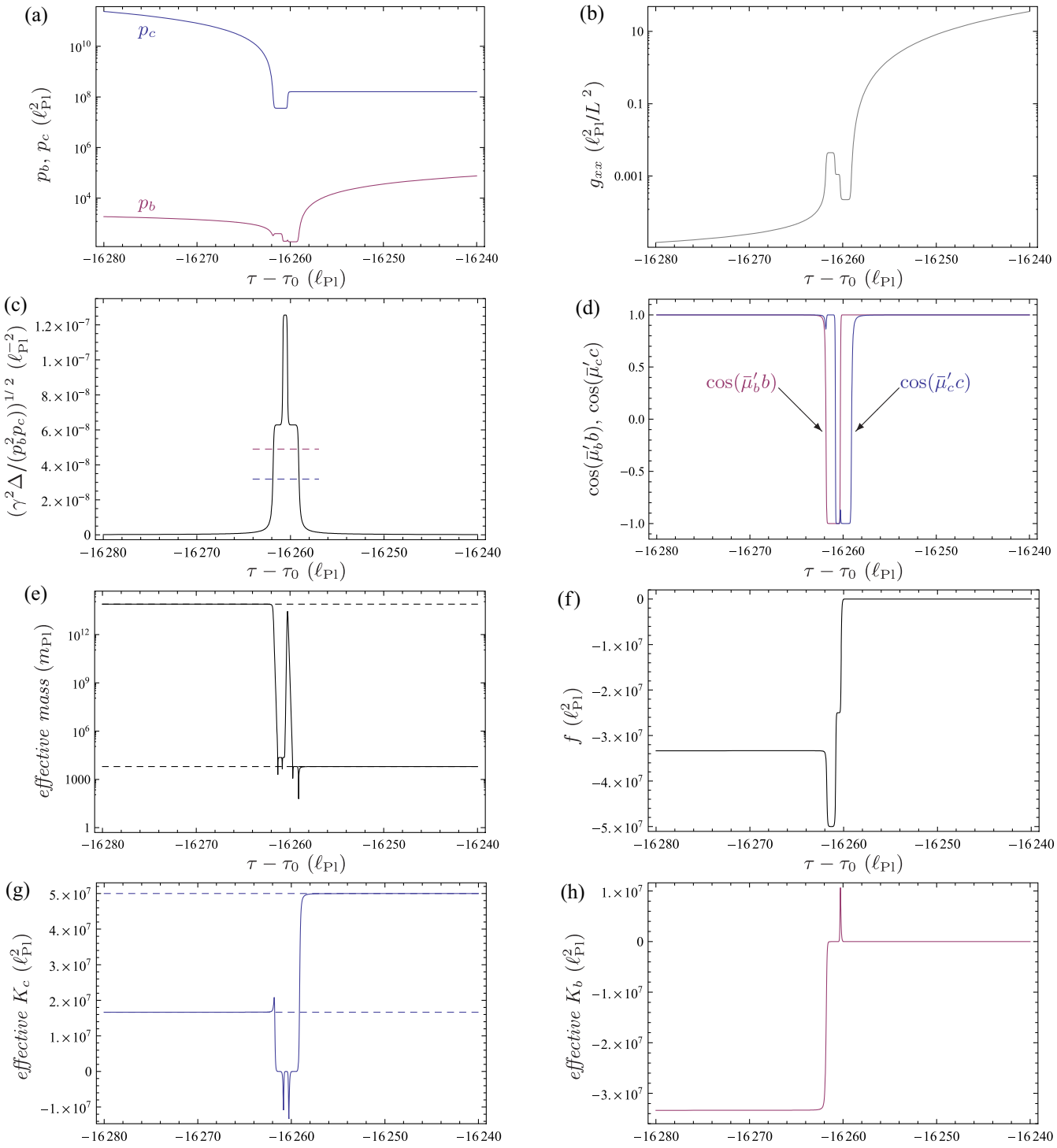

FIG. 4 (color online). Zoom in of the early time bounce in Fig. 3: (a) $p_b(\tau)$ and $p_c(\tau) = g_{\Omega\Omega}(\tau)$. The epochs of bounces in p_b and p_c are very close to each other. (b) $g_{xx}(\tau)$. (c) $\sqrt{\gamma^2\Delta/(p_b^2 p_c)}$, which signals the occurrence of bounces. The conditions of (3.58) and (3.60) are indicated by dashed lines. (d) $\cos(\bar{\mu}_b' b)$ and $\cos(\bar{\mu}_c' c)$, fairly close to each other; both flip signs twice when undergoing the quantum bounce. (e) Effective mass, with the constants M and $\mathfrak{M}^{-1}(M)$ indicated by dashed lines. See (3.67). (f) $f(\tau)$. $f \approx 0$ in the classical cycle on the right and $f \approx -2K_c/3$ on the left. (g) Effective K_c, with the constants K_c and $K_c/3$ indicated by dashed lines. (h) Effective K_b, which becomes 0 on the right of the bounce and $-2K_c/3$ on the left. [For (f)–(h), see (3.52) and the text prior to it for the details.]

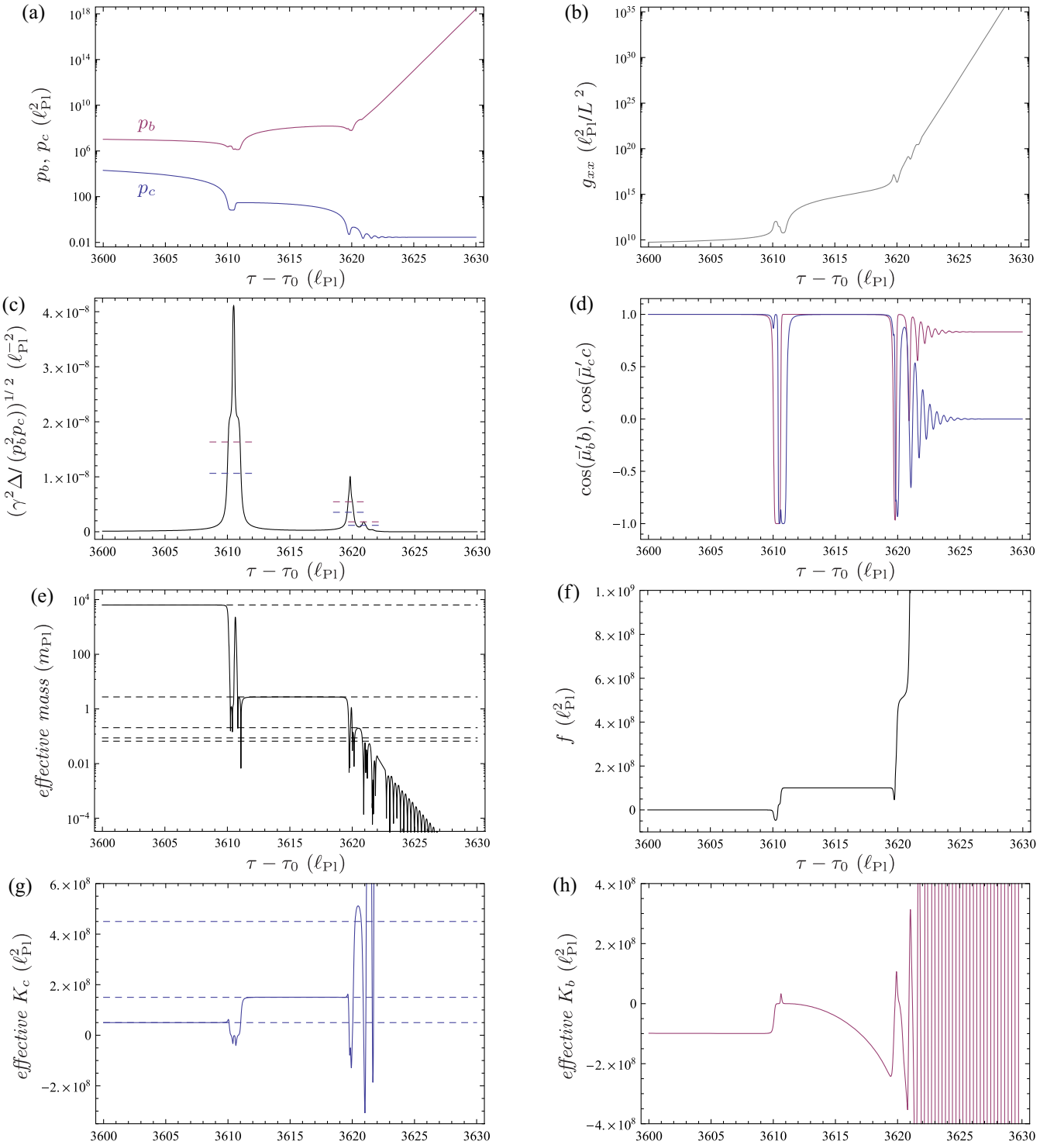

FIG. 5 (color online). Zoom in of the late time bounce in Fig. 3: (a) $p_b(\tau)$ and $p_c(\tau) = g_{\Omega\Omega}(\tau)$. A few classical cycles are connected through quantum bounces. The semiclassicality of these cycles is however less and less established; eventually, p_c descends into a deep Planck regime as $p_c \to \bar{p}_c$ and p_b grows exponentially as $p_b \to \bar{p}_b e^{\kappa\tau}$ with constants given by (3.78) and (3.79). (b) $g_{xx}(\tau)$. (c) $\sqrt{\gamma^2\Delta/(p_b^2 p_c)}$, which signals the occurrence of bounces. The conditions of (3.58) and (3.60) with corresponding effective K_c are indicated by dashed lines. (d) $\cos(\bar{\mu}_b' b)$ and $\cos(\bar{\mu}_c' c)$, which are close to $+1$ in classical cycles but oscillate rapidly when the semiclassicality breaks down and eventually $\cos(\bar{\mu}_c' c) \to 0$ and $\cos(\bar{\mu}_b' b) \to \cos\beta$ as given in (3.77). (e) Effective mass, with the constants M, $\mathfrak{M}(M)$, $\mathfrak{M}(\mathfrak{M}(M))$, ...indicated by dashed lines. See (3.67). (f) $f(\tau)$, which becomes constant in each classical cycle. (g) Effective K_c, with the constants K_c, $3K_c$, and 3^2K_c indicated by dashed lines. (h) Effective K_b. [For (f)–(h), see (3.52) and the text prior to it for the details.]

$\cos(\bar{\mu}_c' c) = 0$, $\sin(\bar{\mu}_c' c) = 1$], $\bar{\mu}_b' b = \beta$ being a constant and consequently

$$\kappa = \frac{1}{\gamma\sqrt{\Delta}}\cos\beta(\sin\beta + 1). \tag{3.70}$$

Substituting these into (3.36) and (3.38), we have

$$\frac{db}{d\tau} = 0 \Rightarrow b = \bar{b} \text{ being a constant,} \tag{3.71}$$

$$\frac{dc}{d\tau} = \bar{p}_b e^{\kappa\tau}\left[\frac{\beta\cos\beta(\sin\beta + 1)}{\gamma\Delta\sqrt{\bar{p}_c}} + \frac{\gamma}{\bar{p}_c^{3/2}}\right] \Rightarrow c = \bar{c}e^{\kappa\tau} \text{ with a constant } \bar{c}. \tag{3.72}$$

Additionally, $(2n + 1/2)\pi = \bar{\mu}_c' c = c\sqrt{\bar{p}_c\Delta}/p_b$ yields

$$\bar{c} = \left(2n\pi + \frac{\pi}{2}\right)\frac{\bar{p}_b}{\sqrt{\bar{p}_c\Delta}}. \tag{3.73}$$

Taking (3.73) into (3.72), we have

$$\left(2n\pi + \frac{\pi}{2}\right)\kappa = \frac{\beta\cos\beta(\sin\beta + 1)}{\gamma\sqrt{\Delta}} + \frac{\gamma\sqrt{\Delta}}{\bar{p}_c}. \tag{3.74}$$

Finally, the Hamiltonian constraint (3.34) reads as

$$2\sin\beta + \sin^2\beta + \frac{\Delta\gamma^2}{\bar{p}_c} = 0. \tag{3.75}$$

Summing up (3.70), (3.74), and (3.75), we have

$$\left(2n\pi + \frac{\pi}{2}\right)\cos\beta(\sin\beta + 1) = \beta\cos\beta(\sin\beta + 1) - 2\sin\beta - \sin^2\beta, \tag{3.76}$$

the numerical solution of which is given by

$$\beta \simeq 2n\pi - 0.587233, \qquad \cos\beta \simeq 0.832477. \tag{3.77}$$

By (3.70) and (3.75), this leads to

$$\bar{p}_c \simeq 1.24823\gamma^2\Delta \simeq 0.0280788\ell_{\mathrm{Pl}}^2 \tag{3.78}$$

and

$$\kappa \simeq 0.371235\gamma^{-1}\Delta^{-1/2} \simeq 2.47518\ell_{\mathrm{Pl}}^{-1}. \tag{3.79}$$

These precisely agree with the asymptotic behaviors shown in Figs. 5(a) and 5(d). Also note that (3.78) is fairly close to the lower bound in (3.35).[12]

Finally, as to the issue of dependence on I, (3.40) and (3.41) imply that the quantities $\bar{\mu}_b' b$, $\bar{\mu}_c' c$ depend only on $p_b^{-1}dp_b/d\tau$, $p_c^{-1}dp_c/d\tau$ and thus are independent of I (recall $p_b \propto L$, $p_c \propto L^0$). Consequently, (3.43) and (3.44) tell us that K_c, $\bar{K}_b$, and f all scale as $\propto L$. Therefore, the phenomenological dynamics given by (3.53) and (3.54) is completely independent of the choice of I as is the classical dynamics. In particular, the choice of I has no effect on the conditions of bounce occurrence in (3.58) and (3.60). This is a desirable feature that the $\bar{\mu}$ scheme does not have. (However, if we further impose the quantum corrections on the eigenvalue of the cotriad operator $\hat{\omega}_c$, this invariance is broken again.)

IV. SCALING SYMMETRY

We have noted that the classical dynamics and the phenomenological dynamics in the $\bar{\mu}'$ scheme are both completely independent of the choice of the finite sized interval I, whereas the phenomenological dynamics in the $\bar{\mu}$ scheme reacts to the physical size of I. This can be rephrased in terms of the scaling symmetry[13]; that is, the classical dynamics and the $\bar{\mu}'$-scheme phenomenological dynamics are invariant under the following scaling:

$$\begin{aligned} &p_b,\ p_c \to l p_b,\ p_c, \qquad b,\ c \to b,\ lc, \\ &K_c \to lK_c, \qquad M \to M. \end{aligned} \tag{4.1}$$

(Note that the scaling for K_c should be accompanied by the same scaling on K_b in classical dynamics and on $\bar{K}_b'$ as well as f in the $\bar{\mu}'$ scheme; that is K_b, $\bar{K}_b'$, $f \to lK_b$, $l\bar{K}_b'$, and lf.) On the other hand, the $\bar{\mu}$ scheme does not respect this scaling. In particular, the conditions for bounce occurrence given in (3.27) and (3.28) depend on I while those in (3.58) and (3.60) do not.

This implies that in the $\bar{\mu}$ scheme the choice of I has a physical consequence, and in the language of the no-hair theorem, one extra parameter (M' or K_c) is required to completely characterize the extended Schwarzschild solution. In the $\bar{\mu}'$ scheme, by contrast, the choice of I is physically irrelevant, and the no-hair theorem holds the same.

Additionally, the classical dynamics also admits the symmetries given by

$$\begin{aligned} &\tau \to \eta\tau, \qquad \gamma \to \xi\gamma, \qquad p_b,\ p_c \to \eta^2 p_b,\ \eta^2 p_c, \\ &b,\ c \to \xi b,\ \xi c, \qquad K_c \to \eta^2 K_c, \qquad M \to \eta M. \end{aligned} \tag{4.2}$$

The scaling symmetry regarding $\gamma \to \xi\gamma$ is expected, since the Barbero-Immirzi parameter γ has no effect on

[12]It was claimed in [15] that the $\bar{\mu}$-scheme phenomenological dynamics extends a classical Schwarzschild black hole to a patch of a nonsingular charged Nariai universe, which gives constant p_c. However, a closer look suggests that the extended part is *not* a patch of the classical Nariai universe but instead represents the quantum spacetime which *formally* exhibits a Nariai-type metric, as the asymptotic constant $\bar{p}_c$ is in the deep Planck regime ($\lesssim \ell_{\mathrm{Pl}}^2$).

[13]A dynamical system is said to be invariant under a certain scaling if for a given solution $[p_b(\tau), p_c(\tau), b(\tau)$ and $c(\tau)]$ to the dynamics, the rescaled functions also satisfy the equations of motion (i.e., Hamilton equations and vanishing of Hamiltonian constraint). For the classical dynamics, the equations to be satisfied are (2.18), (2.19), (2.20), (2.21), and (2.22); for the $\bar{\mu}$ scheme, (3.10), (3.11), (3.12), (3.13), and (3.14); and for the $\bar{\mu}'$ scheme, (3.36), (3.37), (3.38), (3.39), and (3.46).

the classical dynamics. The scaling symmetry regarding $\tau \to \eta\tau$ is also easy to understand, since there is no temporal scale introduced in the Hamiltonian.[14] However, very surprisingly, the scaling symmetry involving $\tau \to \eta\tau$ is violated for both the $\bar{\mu}$-scheme and the $\bar{\mu}'$-scheme phenomenological dynamics. Curiously, this symmetry is restored if $\tau \to \eta\tau$ is accompanied by $\gamma \to \xi\gamma$ and one extra scaling is also imposed at the same time:

$$\Delta \to \xi^{-2}\eta^2\Delta. \tag{4.3}$$

This intriguing observation seems to suggest, albeit speculatively, that in the context of quantum gravity the fundamental scale (area gap) in spatial geometry gives rise to a temporal scale via the nonlocality of quantum gravity (i.e., using holonomies) and the Barbero-Immirzi parameter γ somehow plays the role bridging the scalings in time and space. [This reminds us that, in LQG, the precise value of the area gap Δ is proportional to γ, and γ is also the parameter which relates the *intrinsic* geometry (encoded by spin connection Γ_a^i) with the *extrinsic* curvature ($K_a{}^i$) via $A_a{}^i = \Gamma_a^i - \gamma K_a{}^i$.] Moreover, taking (4.2) and (4.3) into (3.66), we also have

$$\mathfrak{M} \to \eta\mathfrak{M}. \tag{4.4}$$

The above observations for scaling symmetry draw close parallels to those in [10,16] for the phenomenological dynamics of LQC in the Bianchi I and Kantowski-Sachs models. Because of the absence of any matter content, however, some implications thereof are missing here; particularly, the occurrence of bounces is no longer indicated by the (directional) matter energy density. Nevertheless, if we define "energy density" ρ and "directional densities" ρ_b, ρ_c as

$$\rho := \frac{K_c^2}{8\pi G p_b^2 p_c}, \qquad \rho_b := \frac{K_c^2}{8\pi G p_b^3}, \qquad \rho_c := \frac{K_c^2}{8\pi G p_c^3}, \tag{4.5}$$

then according to (3.27), (3.28), (3.58), and (3.60), the bounces can still be said to take place whenever energy density or directional density approaches the Planckian density $\rho_{\mathrm{Pl}} := (8\pi G\gamma^2\Delta)^{-1}$ (up to a numerical factor). This not only paraphrases the condition of bounce occurrence in a universal form as (generalized) energy density being the indicator for the bounce but also suggests that we should put the anisotropic shear on the equal footing as matter content and take into account the energy density arising from it.[15] From this perspective, the ideas of relational interpretation of quantum mechanics remarked in [10,16] can be carried over even without matter content.

Unfortunately, all the scaling symmetries break down in the detailed construction for the quantum geometry of the Schwarzschild interior. The fundamental quantum theory only respects the scaling symmetries at the leading order. This is due to the fact that the quantum evolution in the fundamental theory is governed by a difference equation, in which the step size of difference introduces an additional scale in the deep Planck regime [12]. In fact, already in the level of phenomenological dynamics, the scaling symmetries are violated if we further take into account the loop quantum corrections on the cotriad component ω_c. For the fundamental quantum theory, if we take the aforementioned symmetries seriously, we should revise the detailed construction to have the step size in the difference equation scale accordingly such that the symmetries are respected.

V. SUMMARY AND DISCUSSION

To summarize, we list the important facts for the classical dynamics, $\bar{\mu}$-scheme, and $\bar{\mu}'$-scheme phenomenological dynamics in Table I. The conjectured Penrose diagrams are depicted in Fig. 6. In the following, the main results are restated and their implications are discussed.

In the $\bar{\mu}$-scheme phenomenological dynamics, the classical singularity is resolved and replaced by the quantum bounce, which bridges the black hole interior with the interior of a white hole. The black hole mass M is different from the white hole mass M' in general while the constant K_c flips signs but its magnitude is unchanged.

On the other hand, in the $\bar{\mu}'$-scheme phenomenological dynamics, the classical black hole singularity is resolved and the event horizon is diffused by the quantum bounce. Jumping over the quantum bounce, the classical black hole with K_c and M gives birth to a baby black hole with $3K_c$ and the decreased mass $\mathfrak{M}(M)$ in the consecutive classical cycle. The baby black hole also brings forth its own baby and this scenario continues, giving the extended spacetime fractal structure, until eventually p_b grows exponentially and p_c asymptotes to a fixed value in the deep Planck regime, where the spacetime is essentially quantum mechanical and the semiclassical analysis could be questioned.

[14]For the Bianchi I cosmology studied in [10], a different scaling $p_I \to p_I$ with $c_I \to \eta^{-1}c_I$ is chosen to respect the symmetry regarding $\tau \to \eta\tau$. This alternative scaling does not work in the case of Kantowski-Sachs spacetime, since it violates the Hamiltonian constraint (2.17). That is to say, the presence of the spatial curvature [i.e., the $\gamma^2 p_b^2$ term in the bracket in (2.17)] ties the temporal scale with the spatial scale; as a result, only the scaling $p_b, p_c \to \eta^2 p_b, \eta^2 p_c$ (which gives the spatial direction the same scaling as in the temporal direction) with $b, c \to b, c$ preserves the symmetry.

[15]As remarked in Sec. II.B of [16], the dynamics with Kantowski-Sachs symmetry closely resembles that in the Bianchi I model, implying that K_c and K_b characterize anisotropic shear and the Hamiltonian constraint can be understood as the relation which relates anisotropy with spatial curvature (and matter energy if any). Moreover, it has been shown in Appendix B of [9] that the anisotropic shear behaves as a kind of anisotropic matter: the quantities defined in (4.5) can be considered as the "energy density of the classical anisotropic shear" (portioned to the specific direction).

TABLE I. Summary of the classical dynamics, $\bar{\mu}$-scheme, and $\bar{\mu}'$-scheme phenomenological dynamics.

Classical dynamics	Phenomenology in $\bar{\mu}$ scheme	Phenomenology in $\bar{\mu}'$ scheme
$2\pi p_b = 2\pi L\sqrt{g_{xx}g_{\Omega\Omega}} = \mathbf{A}_{x\phi} = \mathbf{A}_{x\theta}$	$2\pi p_b = 2\pi L\sqrt{g_{xx}g_{\Omega\Omega}} = \mathbf{A}_{x\phi} = \mathbf{A}_{x\theta}$	$2\pi p_b = 2\pi L\sqrt{g_{xx}g_{\Omega\Omega}} = \mathbf{A}_{x\phi} = \mathbf{A}_{x\theta}$
$\pi p_c = \pi g_{\Omega\Omega} = \mathbf{A}_{\theta\phi}$	$\pi p_c = \pi g_{\Omega\Omega} = \mathbf{A}_{\theta\phi}$	$\pi p_c = \pi g_{\Omega\Omega} = \mathbf{A}_{\theta\phi}$
$b = \gamma \frac{d}{d\tau}\sqrt{g_{\Omega\Omega}} = \frac{\gamma}{2p_c^{1/2}}\frac{dp_c}{d\tau}$	$\frac{\sin(\bar{\mu}_b b)}{\bar{\mu}_b} = \frac{1}{\cos(\bar{\mu}_c c)}\frac{\gamma}{2p_c^{1/2}}\frac{dp_c}{d\tau}$	$\frac{\sin(\bar{\mu}'_b b)}{\bar{\mu}'_b} = \frac{1}{\cos(\bar{\mu}'_c c)}\frac{\gamma}{2p_c^{1/2}}\frac{dp_c}{d\tau}$
$c = \gamma\frac{d}{d\tau}(L\sqrt{g_{xx}}) = \frac{\gamma}{p_c^{1/2}}\frac{dp_b}{d\tau} - \frac{\gamma p_b}{2p_c^{3/2}}\frac{dp_c}{d\tau}$	$\frac{\sin(\bar{\mu}_c c)}{\bar{\mu}_c} = \frac{1}{\cos(\bar{\mu}_b b)}\frac{\gamma}{p_c^{1/2}}\frac{dp_p}{d\tau} - \frac{1}{\cos(\bar{\mu}_c c)}\frac{\gamma p_b}{2p_c^{3/2}}\frac{dp_c}{d\tau}$	$\frac{\sin(\bar{\mu}'_c c)}{\bar{\mu}'_c} = \frac{1}{\cos(\bar{\mu}'_b b)}\frac{\gamma}{p_c^{1/2}}\frac{dp_p}{d\tau} - \frac{1}{\cos(\bar{\mu}'_c c)}\frac{\gamma p_b}{2p_c^{3/2}}\frac{dp_c}{d\tau}$
$p_c c = \gamma K_c$	$p_c\frac{\sin(\bar{\mu}_c c)}{\bar{\mu}_c c} = \gamma K_c$	$p_c c = \gamma[K_c + f(t'')]$
$p_b b = \gamma K_b(t')$	$p_b\frac{\sin(\bar{\mu}_b b)}{\bar{\mu}_b b} = \gamma \bar{K}_b(t')$	$p_b b = \gamma[\bar{K}'_b(t'') + f(t'')]$
$2K_bK_c + K_b^2 + p_b^2 = 0$	$2\bar{K}_bK_c + \bar{K}_b^2 + p_b^2 = 0$	$2\sin(\sqrt{\frac{\Delta\gamma^2}{p_b^2p_c}}(\bar{K}'_b + f))\sin(\sqrt{\frac{\Delta\gamma^2}{p_b^2p_c}}(K_c + f)) + \sin^2(\sqrt{\frac{\Delta\gamma^2}{p_b^2p_c}}(\bar{K}'_b + f)) + \frac{\Delta\gamma^2}{p_c} = 0$
$\frac{1}{p_c}\frac{dp_b}{dt'} = \frac{\mathbf{V}}{4\pi p_c}\frac{dp_c}{d\tau} = 2K_b(t')$	$\frac{1}{p_c}\frac{dp_c}{dt'} = 2\cos(\bar{\mu}_c c)\bar{K}_b(t')$	$\frac{1}{p_c}\frac{dp_c}{dt'} = 2\sqrt{\frac{p_b^2p_c}{\gamma^2\Delta}}\cos(\sqrt{\frac{\gamma^2\Delta}{p_b^2p_c}}(K_c + f)) \times \sin(\sqrt{\frac{\gamma^2\Delta}{p_b^2p_c}}(\bar{K}'_b + f))$
$\frac{1}{p_b}\frac{dp_b}{dt'} = \frac{\mathbf{V}}{4\pi p_c}\frac{dp_b}{d\tau} = K_b(t') + K_c$	$\frac{1}{p_b}\frac{dp_b}{dt'} = \cos(\bar{\mu}_b b)[\bar{K}_b(t') + K_c]$	$\frac{1}{p_b}\frac{dp_b}{dt'} = \sqrt{\frac{p_b^2p_c}{\gamma^2\Delta}}\cos(\sqrt{\frac{\gamma^2\Delta}{p_b^2p_c}}(\bar{K}'_b + f)) \times [\sin(\sqrt{\frac{\gamma^2\Delta}{p_b^2p_c}}(\bar{K}'_b + f)) + \sin(\sqrt{\frac{\gamma^2\Delta}{p_b^2p_c}}(K_c + f))]$
$\frac{dK_b}{dt'} = \frac{\mathbf{V}}{4\pi}\frac{dK_b}{d\tau} = -p_b^2$	$\frac{d\bar{K}_b}{dt'} = -\cos(\bar{\mu}_b b)p_b^2$	$\frac{d\bar{K}'_b}{dt'} = -p_b^2$
$p_c,\ p_b \to 0$ toward classical singularity.	p_c bounces whenever $p_c = (\gamma^2K_c^2\Delta)^{1/3}$;	p_c bounces around the moment when $\frac{\gamma^2\Delta}{p_b^2p_c} \approx \frac{2(3-\sqrt{3})}{(\bar{K}'_b - K_c)^2} \approx \begin{cases}\frac{2(3-\sqrt{3})}{9K_c^2},\\ \frac{2(3-\sqrt{3})}{K_c^2}.\end{cases}$
$p_c \to 4G^2M^2,\ p_b \to 0$ toward event horizon.	p_b bounces whenever $p_b \approx (4\gamma^2K_c^2\Delta)^{1/3}$.	p_b bounces around the moment when $\frac{\gamma^2\Delta}{p_b^2p_c} \approx \frac{6}{(\bar{K}'_b - K_c)^2} \approx \begin{cases}\frac{6}{3K_c^2},\\ \frac{6}{K_c^2}\end{cases}$
	Epochs of bounces in p_b and p_c could be very separate.	p_b, p_c bounce roughly around the same moments.
No quantum bounce. K_c fixed. M fixed.	Classical singularity is resolved by the quantum bounce, which bridges the classical black hole with a classical white hole: $K_c \leftrightarrow -K_c$, $M \leftrightarrow M'$.	Classical singularity is resolved and event horizon is diffused; quantum bounces conjoin classical cycles of black holes: $\cdots \leftrightarrow 3^{-1}K_c \leftrightarrow K_c \leftrightarrow 3K_c \leftrightarrow \cdots$, $\cdots \leftrightarrow \mathfrak{M}^{-1}(M) \leftrightarrow M \leftrightarrow \mathfrak{M}(M) \leftrightarrow \cdots$ Eventually, p_c descends into deep Planck regime while p_b grows exponentially.
Symmetry of scaling:	Symmetry of scaling:	Symmetry of scaling:
$\tau \to \eta\tau$	$\tau \to \eta\tau$	$\tau \to \eta\tau$
$\gamma \to \xi\gamma$	$\gamma \to \xi\gamma$	$\gamma \to \xi\gamma$
$p_b,\ p_c \to l\eta^2 p_b,\ \eta^2 p_c$	$p_b,\ p_c \to \eta^2 p_b,\ \eta^2 p_c$	$p_b,\ p_c \to l\eta^2 p_b,\ \eta^2 p_c$
$b,\ c \to \xi b,\ l\xi c$	$b,\ c \to \xi b,\ \xi c$	$b,\ c \to \xi b,\ l\xi c$
$K_c \to l\eta^2 K_c$	$K_c \to \eta^2 K_c$	$(K_c + f) \to l\eta^2(K_c + f)$
$M \to \eta M$	$M \to \eta M$	$M,\ \mathfrak{M} \to \eta M,\ \eta\mathfrak{M}$
	$\Delta \to \xi^{-2}\eta^2\Delta$	$\Delta \to \xi^{-2}\eta^2\Delta$

With regard to the finite sized interval $\mathcal{I}$ chosen to make sense of the Hamiltonian formalism, the phenomenological dynamics in the $\bar{\mu}$ scheme depends on the choice of $\mathcal{I}$. Particularly, given the black hole mass M, the exact value M' of the conjoined white hole depends on $\mathcal{I}$. In the language of the no-hair theorem, two parameters M and M' (or alternatively, say M and K_c) are required to completely characterize the (extended) Schwarzschild solution, although the information of M' is hidden by the horizon and inaccessible (at least semiclassically) to the external

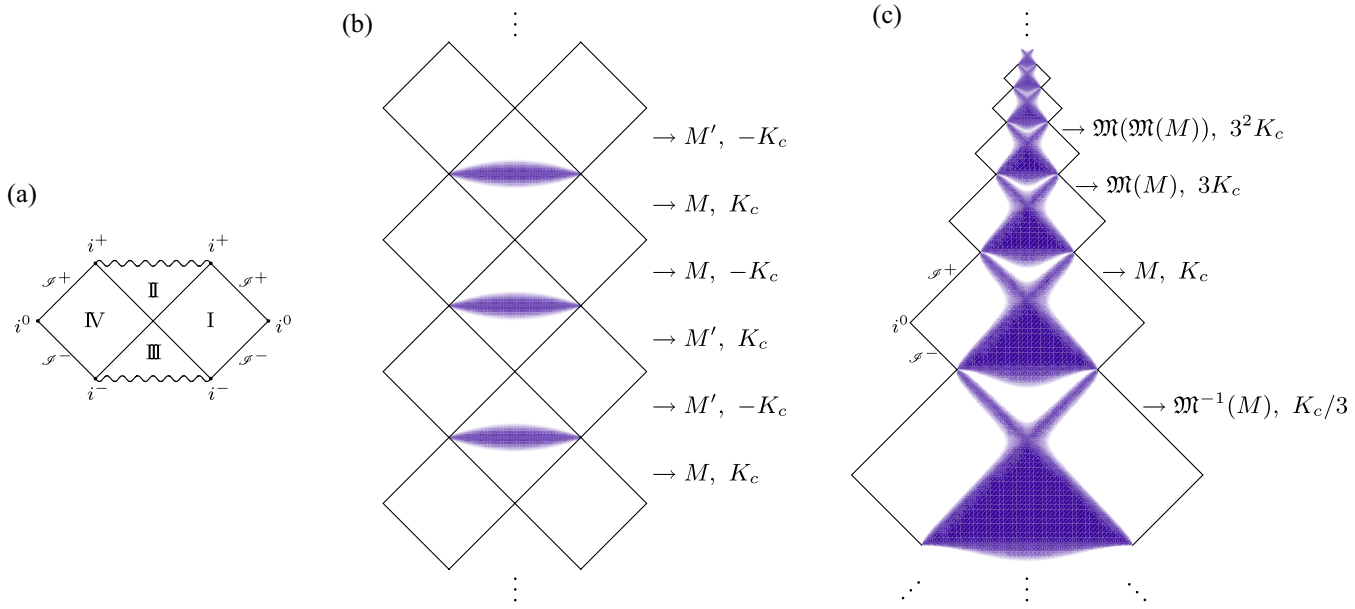

FIG. 6 (color online). (Conjectured) Penrose diagrams: (a) (Maximally extended) classical Schwarzschild spacetime. Region II is the black hole; region III is the white hole; region I is the asymptotically flat region, external to the black hole; and region IV is the other asymptotically flat region. The wiggly lines are the black hole and the white hole singularities. (b) Schwarzschild spacetime in the $\bar{\mu}$ scheme. Both the classical black and white hole singularities are resolved by the quantum bounces (shaded areas), which bridge black holes with white holes. (c) Schwarzschild spacetime in the $\bar{\mu}'$ scheme. The classical black hole singularity is resolved and the event horizon is diffused by the quantum bounce. As a result, jumping over the quantum bounce (shaded area), the black hole gives birth to a baby black hole with increased K_c and drastically decreased mass. This lineage continues until eventually p_b grows exponentially and p_c descends into a constant in the deep Planck regime as the spacetime becomes highly quantum mechanical. [The shaded areas indicate the regions where the quantum effects are significant (the darker the shade, the stronger the quantum effects). The patches for regions I and IV drawn in (b) and (c) are only conjectural.]

observer. By contrast, the phenomenological dynamics in the $\bar{\mu}'$ scheme is completely independent of $\mathcal{I}$ as is the classical dynamics and the no-hair theorem remains unchanged.

In addition to the symmetry related to the choice of $\mathcal{I}$, both schemes admit additional symmetries of scaling, which are suggestive that the fundamental scale (area gap) in spatial geometry may give rise to a fundamental scale in temporal measurement. These symmetries, however, break down in the construction for the fundamental quantum theory.

While the $\bar{\mu}'$ scheme has the advantage that its phenomenological dynamics is independent of $\mathcal{I}$, the fundamental quantum theory of the Schwarzschild interior based on the $\bar{\mu}'$ scheme is difficult to construct. Both the $\bar{\mu}$ and $\bar{\mu}'$ schemes have desirable merits and it is still disputable which one (or yet another possibility) is more faithful to implement the underlying physics of loop quantum geometry. This issue is in the same status as that in the Bianchi I [10] and Kantowsi-Sachs [16] cosmological models. Hopefully, the detailed investigations in this paper on both schemes would help elucidate this issue. However, we should keep in mind that the validity of the phenomenological analysis remains to be justified. Some initial attempt has been made in [22] to construct the semiclassical wave functions in the original μ_o scheme. It would be worthwhile to extend the previous work to the improved ($\bar{\mu}$ or $\bar{\mu}'$) scheme and compare the results with those obtained here.

Meanwhile, it has been suggested [23] and recently analyzed in detail for 2-dimensional black holes [24] that quantum geometry effects may provide a possible mechanism for recovery of information that is classically lost in the process of Hawking evaporation, primarily because the black hole singularity is resolved and consequently the quantum spacetime is sufficiently larger than the classical counterpart. It would be very instructive to study the information paradox in the context of loop quantum geometry of the Schwarzschild black hole, as both resolution of the classical singularity and augmentation of spacetime have been observed at the level of phenomenological dynamics.

Additionally, in the $\bar{\mu}'$ scheme, the quantum effects not only resolve the singularity but also modify the event horizon. The fact that the event horizon is diffused may have an impact on the Hawking evaporation process. However, the homogeneous framework used on this paper only allows us to study the interior of the black hole and it is unclear how exactly the horizon is diffused and pieced together with the exterior (regions I or IV in Fig. 6). In

order to extend the results to cover the whole spacetime, the next step would be to apply the techniques described here to the inhomogeneous formulation of spherically symmetric loop quantum geometry such as was developed in [25,26]. This in turn could enable us to study the collapsing scenario of loop quantum black holes.

ACKNOWLEDGMENTS

This work was supported in part by the Eberly Research Funds of The Pennsylvania State University.

APPENDIX: PHENOMENOLOGICAL DYNAMICS IN THE μ_o SCHEME

One of the virtues of the improved strategy ($\bar{\mu}$ or $\bar{\mu}'$ scheme) in both the isotropic and Bianchi I models of LQC is to fix the serious drawback in the original strategy (μ_o scheme), whereby the critical value of matter density ρ_ϕ (in the isotropic model) or of directional densities ϱ_I (in the Bianchi I model) at which the bounce occurs can be made arbitrarily small by increasing the momentum p_ϕ of the matter field, thereby giving the wrong semiclassical behavior [4,8,10]. In the case of the Schwarzschild interior, without the reference of matter content, it is not clear whether the μ_o scheme is problematic in regard to semiclassicality. For comparison, the phenomenological dynamics in the μ_o scheme is presented here.

In the phenomenological theory of the μ_o scheme, we take the prescription to replace c and b with $\sin(\mu_c^o c)/\mu_c^o$ and $\sin(\mu_b^o b)/\mu_b^o$ by introducing the *fixed* numbers μ_c^o and μ_b^o for discreteness. Analogous to (3.2), we have the effective (rescaled) Hamiltonian constraint:

$$H'_{\mu_o} = -\frac{1}{2G\gamma}\left\{2\frac{\sin(\mu_b^o b)}{\mu_b^o}\frac{\sin(\mu_c^o c)}{\mu_c^o}p_b p_c + \left(\frac{\sin(\mu_b^o b)}{\mu_b^o}\right)^2 p_b^2 + \gamma^2 p_b^2\right\}. \tag{A1}$$

To get an idea where the quantum corrections become appreciable, employing the classical solution given by (2.29), (2.33), and (2.34), we estimate the quantities $\mu_b^o b$ and $\mu_c^o c$:

$$\mu_b^o b = \gamma\mu_b^o\frac{K_b}{p_b} \to \begin{cases}\infty & \text{as } t' \to \infty,\\ 0 & \text{as } t' \to -\infty,\end{cases} \tag{A2}$$

$$\mu_c^o c = \gamma\mu_c^o\frac{K_c}{p_c} \to \begin{cases}\infty & \text{as } t' \to \infty,\\ \frac{\gamma\mu_c^o K_c}{4G^2M^2} & \text{as } t' \to -\infty.\end{cases} \tag{A3}$$

This suggests that the quantum corrections are significant near the classical singularity and negligible on the horizon provided that

$$K_c \ll \frac{4G^2M^2}{\gamma\mu_c^o}, \tag{A4}$$

which can always be satisfied if we choose $\mathcal{I}$ small enough for a given M.

The equations of motion are given by the Hamiltonian constraint $H'_{\mu_o} = 0$ and Hamilton's equations:

$$\frac{dc}{dt'} = \{c, H'_{\mu_o}\} = 2G\gamma\frac{\partial H'_{\mu_o}}{\partial p_c} = -2\gamma^{-1}p_b\frac{\sin(\mu_b^o b)}{\mu_b^o}\frac{\sin(\mu_c^o c)}{\mu_c^o}, \tag{A5}$$

$$\frac{dp_c}{dt'} = \{p_c, H'_{\mu_o}\} = -2G\gamma\frac{\partial H'_{\mu_o}}{\partial c} = 2\gamma^{-1}p_b p_c\cos(\mu_c^o c)\frac{\sin(\mu_b^o b)}{\mu_b^o}, \tag{A6}$$

$$\frac{db}{dt'} = \{b, H'_{\mu_o}\} = G\gamma\frac{\partial H'_{\mu_o}}{\partial p_b} = -\gamma^{-1}p_c\frac{\sin(\mu_b^o b)}{\mu_b^o}\frac{\sin(\mu_c^o c)}{\mu_c^o} - \gamma^{-1}p_b\left[\frac{\sin(\mu_b^o b)}{\mu_b^o}\right]^2 - \gamma p_b, \tag{A7}$$

$$\frac{dp_b}{dt'} = \{p_b, H'_{\mu_o}\} = -G\gamma\frac{\partial H'_{\mu_o}}{\partial b} = \gamma^{-1}p_b\cos(\mu_b^o b)\left[p_b\frac{\sin(\mu_b^o b)}{\mu_b^o} + p_c\frac{\sin(\mu_c^o c)}{\mu_c^o}\right], \tag{A8}$$

which follow

$$\frac{d}{dt'}\left[p_c\frac{\sin(\mu_c^o c)}{\mu_c^o}\right] = 0 \Rightarrow p_c\frac{\sin(\mu_c^o c)}{\mu_c^o} = \gamma K_c \tag{A9}$$

and

$$p_c\frac{\sin(\mu_b^o b)}{\mu_b^o} =: \gamma K_b^o(t'), \qquad \frac{dK_b^o}{dt'} = -\gamma^2 p_b^2\cos(\mu_b^o b). \tag{A10}$$

These are exactly the same as (3.17), (3.18), (3.19), and (3.20) except that the discreteness variables $\bar{\mu}_c$ and $\bar{\mu}_b$ are now replaced by μ_c^o and μ_b^o.

Therefore, exploiting the close resemblance between the $\bar{\mu}$ scheme and the μ_o scheme, we can readily repeat the calculation we did in Sec. III A and obtain the differential equations [cf. (3.22), (3.23), and (3.24)]:

$$\frac{dK_b^o}{dt'} = \cos(\mu_b^o b)(2K_b^o K_c^o + \bar{K}_b^2 - K_\phi^2), \tag{A11}$$

$$\frac{1}{p_c}\frac{dp_c}{dt'} = 2\cos(\mu_c^o c)K_b^o, \tag{A12}$$

$$\frac{1}{p_b}\frac{dp_b}{dt'} = \cos(\mu_b^o b)[K_b^o + K_c], \tag{A13}$$

where

$$\cos(\mu_c^o c) = \pm[1 - \sin^2\mu_c^o c]^{1/2} = \pm\left[1 - \left(\frac{\gamma\mu_c^o K_c}{p_c}\right)^2\right]^{1/2}, \tag{A14}$$

$$\cos(\mu_b^o b) = \pm[1 - \sin^2\mu_b^o b]^{1/2} = \pm\left[1 - \left(\frac{\gamma\mu_c^o K_b^o}{p_b}\right)^2\right]^{1/2}, \tag{A15}$$

which give the bouncing solution similar to that given in the $\bar{\mu}$-scheme phenomenological dynamics except that the exact conditions at which the bounce takes place are given differently by [cf. (3.27) and (3.28)]

$$p_c = \gamma\mu_c^o K_c \ll 4G^2M^2, \tag{A16}$$

$$p_b = \gamma\mu_b^o|K_b^o| \approx 2\gamma\mu_c^o K_c \ll 8G^2M^2. \tag{A17}$$

The phenomenological dynamics of the μ_o scheme closely resembles that of the $\bar{\mu}$ scheme. The classical singularity is resolved and replaced by the quantum bounce, which bridges a black hole interior with a white hole interior. The dynamics also depends on the choice of $\mathcal{I}$. The exact solution with $\mu_b^o = \mu_c^o = \delta$ can be found in [14,15].

[1] M. Bojowald, Living Rev. Relativity **8**, 11 (2005).
[2] A. Ashtekar, T. Pawlowski, and P. Singh, Phys. Rev. D **73**, 124038 (2006).
[3] A. Ashtekar, T. Pawlowski, and P. Singh, Phys. Rev. Lett. **96**, 141301 (2006).
[4] A. Ashtekar, T. Pawlowski, and P. Singh, Phys. Rev. D **74**, 084003 (2006).
[5] A. Ashtekar, T. Pawlowski, P. Singh, and K. Vandersloot, Phys. Rev. D **75**, 024035 (2007).
[6] K. Vandersloot, Phys. Rev. D **75**, 023523 (2007).
[7] D. W. Chiou, Phys. Rev. D **75**, 024029 (2007).
[8] D. W. Chiou, arXiv:gr-qc/0703010.
[9] D. W. Chiou and K. Vandersloot, Phys. Rev. D **76**, 084015 (2007).
[10] D. W. Chiou, Phys. Rev. D **76**, 124037 (2007).
[11] L. Modesto, Int. J. Theor. Phys. **45**, 2235 (2006).
[12] A. Ashtekar and M. Bojowald, Classical Quantum Gravity **23**, 391 (2006).
[13] L. Modesto, Classical Quantum Gravity **23**, 5587 (2006).
[14] L. Modesto, arXiv:gr-qc/0611043.
[15] C. G. Boehmer and K. Vandersloot, Phys. Rev. D **76**, 104030 (2007).
[16] D. W. Chiou, Phys. Rev. D **78**, 044019 (2008).
[17] P. Singh and K. Vandersloot, Phys. Rev. D **72**, 084004 (2005).
[18] M. Bojowald, Phys. Rev. D **75**, 081301 (2007).
[19] V. Taveras, arXiv:0807.3325.
[20] D. W. Chiou, "Effective Equations of Motion in Bianchi I Quantum Cosmology" (unpublished).
[21] M. Bojowald, D. Cartin, and G. Khanna, Phys. Rev. D **76**, 064018 (2007).
[22] D. Cartin and G. Khanna, Phys. Rev. D **73**, 104009 (2006).
[23] A. Ashtekar and M. Bojowald, Classical Quantum Gravity **22**, 3349 (2005).
[24] A. Ashtekar, V. Taveras, and M. Varadarajan, Phys. Rev. Lett. **100**, 211302 (2008).
[25] M. Campiglia, R. Gambini, and J. Pullin, Classical Quantum Gravity **24**, 3649 (2007).
[26] M. Bojowald, Classical Quantum Gravity **21**, 3733 (2004).